

Impacts of Parameterized Langmuir Turbulence and Nonbreaking Wave Mixing in Global Climate Simulations

YALIN FAN

Program in Atmospheric and Oceanic Sciences, Princeton University, and NOAA/Geophysical Fluid Dynamics Laboratory, Princeton, New Jersey

STEPHEN M. GRIFFIES

NOAA/Geophysical Fluid Dynamics Laboratory, Princeton, New Jersey

(Manuscript received 26 September 2013, in final form 24 February 2014)

ABSTRACT

The impacts of parameterized upper-ocean wave mixing on global climate simulations are assessed through modification to Large et al.'s K -profile ocean boundary layer parameterization (KPP) in a coupled atmosphere–ocean–wave global climate model. The authors consider three parameterizations and focus on impacts to high-latitude ocean mixed layer depths and related ocean diagnostics. The McWilliams and Sullivan parameterization (MS2000) adds a Langmuir turbulence enhancement to the nonlocal component of KPP. It is found that the Langmuir turbulence–induced mixing provided by this parameterization is too strong in winter, producing overly deep mixed layers, and of minimal impact in summer. The later Smyth et al. parameterization modifies MS2000 by adding a stratification effect to restrain the turbulence enhancement under weak stratification conditions (e.g., winter) and to magnify the enhancement under strong stratification conditions. The Smyth et al. scheme improves the simulated winter mixed layer depth in the simulations herein, with mixed layer deepening in the Labrador Sea and shoaling in the Weddell and Ross Seas. Enhanced vertical mixing through parameterized Langmuir turbulence, coupled with enhanced lateral transport associated with parameterized mesoscale and submesoscale eddies, is found to be a key element for improving mixed layer simulations. Secondary impacts include strengthening the Atlantic meridional overturning circulation and reducing the Antarctic Circumpolar Current. The Qiao et al. nonbreaking wave parameterization is the third scheme assessed here. It adds a wave orbital velocity to the Reynolds stress calculation and provides the strongest summer mixed layer deepening in the Southern Ocean among the three experiments, but with weak impacts during winter.

1. Introduction

Wind-generated ocean surface gravity waves (OSGWs) [periods $O(1\text{--}10\text{ s})$ and wavelength $O(1\text{--}1000\text{ m})$] play a significant role in many physical processes at the air–sea interface. In particular, they are believed to be a leading-order cause of mixing in the upper ocean through wave breaking and the generation of Langmuir turbulence (Belcher et al. 2012), with this mixing important for momentum, heat, and gas exchange across the air–sea interface.

The transfer of mass, momentum, and energy across the mixed layer provides the source of interior ocean

properties, and the thickness of the mixed layer determines the heat content and mechanical inertia of the layer that directly interacts with the atmosphere. The midlatitude storm regions of both hemispheres are known regions of extreme ocean surface waves (Fan et al. 2012, 2013), which may be a primary factor in generating deep mixed layers in these regions, affecting sea surface temperatures (SSTs), and contributing to the transport and mixing of trace gases. The Southern Ocean is a region of particular importance for surface ocean waves in mixed layer dynamics, where high winds during all seasons and infinite fetch provide unique conditions for extreme ocean waves and strong Langmuir turbulence.

The importance of OSGWs for upper-ocean mixing leads us to consider incorporating a surface wave model into a coupled climate model in order to feed wave information into upper-ocean mixing parameterizations.

Corresponding author address: Yalin Fan, Oceanography Division, Code 7322, Naval Research Laboratory, Stennis Space Center, MS 39529.
E-mail: yalin.fan.ctr@nrlssc.navy.mil

The aim of this paper is to summarize our analysis of centennial-scale climate simulations with this model using three different wave-induced mixing parameterizations.

a. Modeling context for our study

[Delworth et al. \(2006\)](#) noted a positive SST bias at the Southern Ocean when evaluating the Geophysical Fluid Dynamics Laboratory (GFDL) Climate Model, version 2.1 (CM2.1), and attributed this warm bias partly to a positive shortwave radiation bias in the atmosphere. [Dunne et al. \(2012\)](#) also noted a similar SST warm bias in the Southern Ocean when evaluating the GFDL Earth System Model with Modular Ocean Model, version 4 (MOM4), component (ESM2M) and attribute this bias to the similarity between ESM2M and CM2.1. However, the National Center for Atmospheric Research (NCAR) Community Climate System Model, version 4 (CCSM4), has a negative bias in surface radiative forcing and cold bias in SST in the Southern Ocean ([Weijer et al. 2012](#); [Bates et al. 2012](#)). Even so, summertime oceanic mixed layers are biased shallow in both the GFDL and NCAR climate models ([Bates et al. 2012](#); [Dunne et al. 2012, 2013](#)). This common bias in the face of opposing atmospheric biases suggests that the underlying problem is related to ocean processes in the boundary layer, such as mixing, rather than just surface radiative forcing ([Belcher et al. 2012](#); [Sallee et al. 2013](#)). We consider the hypothesis that some of this bias may be related to ocean surface wave-induced mixing.

Third-generation ocean surface gravity wave models [e.g., WAVEWATCH III ([Tolman 1998](#)), the Wave Model (WAM; [Hasselmann et al. 1988](#)), and Simulating Waves Nearshore (SWAN; [Booij et al. 1999](#))] have been developed to simulate and predict wave conditions at sea for both global and regional applications. These spectral models solve for wave energy propagation using the wave action conservation equation. They provide information about variability of surface gravity wave packets rather than individual waves. This approach allows one to accurately model wave conditions using relatively coarse spatial resolution (e.g., hundreds of kilometers) through the use of relatively fine spectral resolution (we chose 24 wave directions and 40 wave frequencies ranging from 0.0285 to 1 Hz). Following from the work of [Fan et al. \(2012, 2013\)](#), we couple WAVEWATCH III to a recently developed GFDL climate model (CM2M discussed in [section 2](#)) in order to investigate the wave-induced mixing hypothesis.

b. Wave-induced mixing parameterizations tested here

Recognizing the potential importance of upper-ocean waves for climate, in particular through impacts on the

ocean mixed layer, modifications have been developed to existing ocean mixing schemes to incorporate effects from surface ocean waves. The present paper considers how three of the proposed schemes impact ocean climate as simulated by a coupled climate model.

The first parameterization we tested is from [McWilliams and Sullivan \(2000\)](#), who were the first to incorporate a Langmuir turbulence parameterization into the *K*-profile ocean boundary layer parameterization (KPP) boundary layer scheme, with their parameterization based on large-eddy simulation (LES) studies. We find that in our climate simulations, this scheme generates too much mixing in the winter and has minimal impact in the summer. We were consequently led to consider the scheme from [Smyth et al. \(2002\)](#), who modified the [McWilliams and Sullivan \(2000\)](#) scheme by adding a stratification effect. Their stratification effect reduced biases they found in simulations of mixing associated with the diurnal cycle. We find that their scheme improves the wintertime mixed layer depth in our climate simulations.

The [Qiao et al. \(2004\)](#) parameterization is the third scheme assessed here. Rather than Langmuir turbulence, their scheme parameterizes effects on mixing from nonbreaking waves, and it shares much in common with the scheme of [Babanin et al. \(2009\)](#). Although considering effects distinct from Langmuir turbulence, and introducing a source for mixing that remains the topic of some uncertainty, we believe it useful to explore the impacts from this scheme, if only to stimulate further investigations to clarify its role in climate modeling. This scheme has most impact in our simulations on deepening the summertime mixed layers, yet it has minimal impact on wintertime mixed layers.

c. Content of this paper

The aim of this paper is to assess the effect of parameterized Langmuir turbulence and nonbreaking waves on global climate simulations. We do so within the framework of “present day” 1990 radiatively forced simulations following the procedure of [Delworth et al. \(2006\)](#). Our results are presented in four sections. The coupled atmosphere–ocean–wave model is described in [section 2](#); simulation results are analyzed in [section 3](#); a summary and discussion are given in [section 4](#), and closing remarks are given in [section 5](#).

2. Methodology

We have developed a fully coupled atmosphere–ocean–wave global climate simulation model at the National Oceanic and Atmospheric Administration (NOAA)/GFDL by incorporating WAVEWATCH III,

the operational wave model developed and used at the National Centers for Environmental Prediction (NCEP) (Tolman 1998), into the GFDL climate model (CM2M based on ESM2M but without interactive biogeochemistry) (Fig. 1). Salient details of CM2M are given in appendix A, with more information in Dunne et al. (2012) and the NOAA/GFDL earth system models documents (<http://www.gfdl.noaa.gov/earth-system-model>). Langmuir turbulence effects have been implemented in CM2M using the proposals from McWilliams and Sullivan (2000) as well as Smyth et al. (2002). Furthermore, the nonbreaking wave effect proposed by Qiao et al. (2004) was also implemented in this coupled system. Details of these parameterizations are provided in sections 2a and 2b.

We configure the wave model with a horizontal grid spacing of 2.5° longitude by 2° latitude corresponding to the atmospheric model resolution. The surface wave spectrum is discretized using 24 directions and 40 intrinsic (relative) frequencies extending from 0.0285 to 1.1726 Hz (wavelength of 1.1–1920 m), with a logarithmic increment of $f(n+1) = 1.1f(n)$, where $f(n)$ is the n th frequency. This relatively fine spectral resolution gives more accurate estimates of global wind sea and swells compared with low spectra resolution configurations like the 40-yr European Centre for Medium-Range Weather Forecasts (ECMWF) Re-Analysis (ERA-40) wave reanalysis [see Fan et al. (2012) for more discussion]. Validation of the annual mean significant wave height (from model years 101 to 200) against corrected ERA-40 gives a spatial correlation of 0.935 with bias within 0.7 m in the midlatitude storm region (not shown). We comment in section 5b on computational costs associated with this wave model configuration.

We describe results from four multicentennial simulations with this coupled model: a control case using the standard K -profile parameterization (Large et al. 1994) and three variations using the alternative mixing parameterizations.

a. Langmuir turbulence parameterization

The dynamical origin of Langmuir circulation is understood as wind-driven shear instability in combination with surface wave influences related to their mean Lagrangian motion, called Stokes drift. The prevailing theoretical interpretation of Langmuir cells is derived by Craik and Leibovich (1976), where they introduced the effect of waves on Eulerian mean flow into the Navier–Stokes equation through a “vortex force” expressed as $\mathbf{u}_s \times \nabla \times \mathbf{u}$ (where \mathbf{u} is the current velocity and \mathbf{u}_s is the Stokes drift velocity). LES studies (Skylvingstad and Denbo 1995; McWilliams et al. 1997; Skylvingstad et al. 2000; McWilliams et al. 2004; Sullivan et al. 2007; McWilliams and Fox-Kemper 2013) found that the

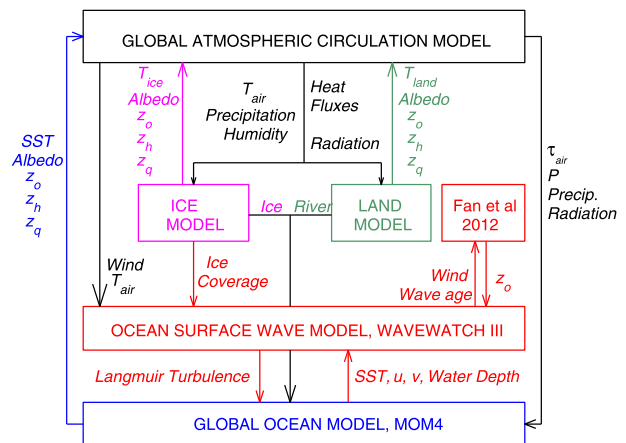


FIG. 1. Schematic diagram of the atmosphere–ocean–wave coupled model. The arrows indicate the prognostic variables that are passed between the model components. In the diagram, z_o , z_q , and z_h , are momentum, latent heat, and sensible heat roughness lengths; T_{air} , T_{ice} , and T_{land} are air, ice, and land temperatures at the surface; τ_{air} is the wind stress; P is the sea level pressure; SST is sea surface temperature; and u and v are ocean current velocity in the longitude and latitude direction.

turbulent energy and mixed-layer depth are enhanced by the vortex force, and the maximum entrainment heat flux $\langle w'\theta' \rangle$ into the mixed layer may increase by a factor of 2–5 when including the vortex force. Stokes drift can also interact with the Coriolis force (Stokes–Coriolis force) and influence the mean Ekman current profile in the ocean boundary layer over most of the globe, especially in high latitudes with high winds (Holm 1996; McWilliams and Restrepo 1999; McWilliams et al. 2004; Polton et al. 2005; Lane et al. 2007). The effects on ocean climate from the Stokes–Coriolis force are beyond the scope of our study.

The ocean component of CM2M uses KPP (Large et al. 1994) to parameterize ocean surface boundary layer turbulence. Of the three wave-induced mixing schemes considered in our study, we consider two that parameterize Langmuir turbulence as implemented through modifications to KPP. Each scheme is tested in CM2M and compared to the control case without a Langmuir turbulence parameterization.

b. McWilliams and Sullivan (2000) parameterization

Through their analysis of LES cases based on surface-wave-averaged, dynamical equations, McWilliams and Sullivan (2000) proposed a modest generalization of KPP to account for both boundary layer depth changes and nonlocal mixing by Langmuir turbulence. Both observations (Smith 1998, 1999) and LES experiments (Skylvingstad et al. 2000) indicate that when Langmuir turbulence is evident, the near-surface, transverse

velocity amplitude varies in direct proportion to the surface Stokes drift. Hence, they argue that the turbulent velocity scale relevant to the mixing rates, W ($W = ku_*/\phi$, where ϕ is the stability function in Monin–Obukhov similarity theory and $k = 0.4$ is the von Kármán constant) in the KPP scheme also has this behavior.

They modified the turbulent velocity scale W by multiplying it by a Langmuir turbulence enhancement factor F_{Lt}

$$F_{Lt} = \left(1 + \frac{L_w}{La^{2\alpha}}\right)^{1/\alpha}, \tag{1}$$

where $La = \sqrt{u_*/|U_s|}$ is the Langmuir number, u_* is the standard friction velocity determined by the boundary momentum stress, $|U_s|$ is the magnitude of the surface Stokes drift velocity calculated by the wave model, and L_w and α are constants. We follow [McWilliams and Sullivan \(2000\)](#) by setting $L_w = 0.08$ and $\alpha = 2$. The corresponding coefficient for the nonlocal flux, $\gamma = -\varphi_\gamma[F_Q(0)/Wh]$, is set to $\varphi_\gamma = 1.08$ ($\varphi_\gamma = 1.0$ for the control). Here, $F_Q(0)$ is the molecular diffusion at $z = 0$ and h is the boundary layer depth. Hereafter, we will refer to this parameterization as MS2000. Note that F_{Lt} equals to 1.0 in the control case where Langmuir turbulence effects are not considered.

The enhancement of W attributable to Langmuir turbulence also enters the calculation of boundary layer depth (BLD) through the bulk Richardson number ([McWilliams and Sullivan 2000](#)),

$$Ri_b = \frac{gh|\Delta(\rho)|}{\rho_0[|\Delta(u)|^2 + W^2]}. \tag{2}$$

Here, ρ is density, u is velocity, and Δ denotes the difference in values between the surface and depth h , and the BLD is equal to the smallest value of depth at which this Richardson number equals a critical value. The angle brackets denote an average in time and horizontal position over the scales of surface waves and boundary layer turbulence.

This adjustment of the KPP scheme results in turbulent velocities proportional to the surface Stokes drift in the regime of small La , where Langmuir turbulence is active. MS2000 show that this modification makes the parameterized KPP flux profiles match those in the LES case fairly well, especially for material properties being transported down from the ocean surface.

c. Smyth et al. (2002) parameterization

When using the MS2000 parameterization to study a westerly wind burst event in the tropical Pacific, [Smyth et al. \(2002\)](#) found that the reduction in daytime warming is insufficient to reproduce their LES results quantitatively, while the application of MS2000 during nocturnal convection causes unrealistically rapid mixing

throughout the mixed layer. [McWilliams and Sullivan \(2000\)](#) also suggested that their parameterization may require modification in regimes of either strong convection or strong wind forcing. Hence, [Smyth et al. \(2002\)](#) proposed to include a stratification effect to the MS2000 parameterization of Langmuir turbulence enhancement by changing the constant L_w in Eq. (1) to a function of L_w and the convective velocity scale w_* :

$$L_w(u_*, w_*) = L_{w0} \left(\frac{u_*^3}{u_*^3 + 0.6w_*^3} \right)^l, \tag{3}$$

where $L_{w0} = 0.15$ and $l = 2$. This modification enhances the effect of Langmuir turbulence in stable conditions (positive buoyancy forcing) and reduces it in convective conditions (negative buoyancy forcing).

[Smyth et al. \(2002\)](#) also added a nonlocal momentum flux in their scheme. This term is set to be zero by [Large et al. \(1994\)](#) given the lack of available data, and thus remains zero in our control case, as well as the MS2000 scheme and the nonbreaking wave parameterization (see below). To be consistent among the four experiments, we neglect the nonlocal momentum flux in our implementation of the [Smyth et al. \(2002\)](#) scheme as well. Studies of a nonlocal momentum term are beyond the scope of our study.

d. Nonbreaking wave parameterization

[Qiao et al. \(2004\)](#) proposed a wave-induced vertical kinematic viscosity and diffusivity through integration of the wave spectrum

$$B_v = l_w^2 \frac{\partial}{\partial z} \left[\iint_k \omega^2 E(\mathbf{k}) \exp(2kz) d\mathbf{k} \right]^{1/2}, \tag{4}$$

where l_w is defined as the mixing length with

$$l_w^2 = \alpha \iint_k E(\mathbf{k}) \exp(2kz) d\mathbf{k}, \tag{5}$$

in which $E(\mathbf{k})$ is the wavenumber spectrum, k is wave-number, z is the vertical coordinate axis upward positive with $z = 0$ at resting ocean surface, and ω is the wave frequency. Also, α is a user tunable coefficient [distinct from that used in Eq. (1)], which is set to 1 in this study following [Qiao et al. \(2004\)](#). The physical basis for this parameterization is that the mixing length of the wave-induced turbulence is proportional to the range of the wave particle displacement, and the vertical eddy diffusivity is a function of the mixing length and the vertical shear of the wave orbital velocity.

e. Coupling

The component models pass fluxes across their interfaces using an exchange grid system. The exchange grid enforces heat, mass, and tracer conservation on the fluxes passed between the component models. Both the atmospheric model and wave model have a time step of 30 min, whereas the ocean model has a 2-h time step. Every 30 min, the atmosphere model exchanges fluxes with the land, ice, and wave model, and the ice model passes ice coverage to the wave model. The coupling between the component models and the ocean model occurs at 2-h intervals, which couples the diurnal cycles of the atmosphere and ocean components.

f. Experiments, initialization, and forcing

Four sets of experiments are conducted in this study. The original CM2M is used in the control experiment; the coupled atmosphere–ocean–wave model with MS2000 Langmuir turbulence parameterization is used in Exp1; the coupled atmosphere–ocean–wave model with Smyth et al. (2002) Langmuir turbulence parameterization is used in Exp2; and the coupled atmosphere–ocean–wave model with Qiao et al. (2004) parameterization is used in Exp3.

To initialize the model, the atmosphere and land initial conditions are taken from the end of a 17-yr run of the atmosphere–land model that uses observed time-varying SSTs and sea ice over the period 1982–98. A 1-yr spinup was performed for the ocean component of the coupled model starting from *World Ocean Atlas 2009* temperature and salinity with zero velocity and zero surface height. The ocean model is forced with heat and water fluxes from an integration of the atmosphere model described above, along with observed wind stress. The wave model was also spun up through a 1-yr simulation starting from a calm sea, and forced with observed wind stress. Outputs from the end of the 1-yr spinups are taken as the initial condition for the coupled run. The sea ice initial conditions are taken from the end of year 10 of a preliminary coupled integration with the same model.

For all integrations, aerosol and trace gas concentrations, insolation, and distribution of land cover types represent 1990 values and do not vary from one year to the next. The specific values used for well-mixed greenhouse gases and solar irradiance are listed in Table 1 in Delworth et al. (2006). Three-dimensional distributions of natural aerosols from sea salt and dust are also prescribed, and there are no aerosols from volcanic sources. Note that sea salt, gas, momentum transfer, and aerosol productions are likely affected by the wave state (Fairall et al. 2003, 2009, 2011; Cavaleri et al. 2012). But these

effects are neglected in this study to focus on the Langmuir turbulence and nonbreaking wave effect on ocean mixing.

The control experiment and Exp2 are run for 500 yr, while Exp1 and Exp3 are run for 200 yr. The time means presented in section 3 are from model years 101 to 200 as in Delworth et al. (2006), with the exception of the ideal age, where years 181–200 are used.

3. Analysis of the simulations

a. Global perspective

The 100-yr mean (from model years 101 to 200) differences in the simulation versus Reynolds observed SST (obtained from the International Research Institute/Lamont-Doherty Earth Observatory Climate Data Library; http://iridl.ldeo.columbia.edu/SOURCES/IGOSS/.nmc/Reyn_SmithOIv2/) are shown in Fig. 2. Model summer and winter mean mixed layer depth (MLD) versus observational MLD (observational estimate are based on the *World Ocean Atlas* obtained from the National Oceanographic Data Center; <http://data.nodc.noaa.gov/woa/WOA09/>) are given in Figs. 3 and 4. Both the observational and model MLD are calculated as the depth at which potential density (referenced to surface) changes by 0.125 kg m^{-3} from its surface values.

The main SST discrepancy between the model results and observations exists in the middle- to high-latitude regions, with a significant SST cold bias in the Northern Hemisphere and SST warm bias in the Southern Hemisphere. The cold biases are related to both an equatorward shift of the westerlies and extensive low cloudiness, and low values of shortwave radiation incident upon the surface (Delworth et al. 2006). Neither of these biases is the focus of our study here. The SST warm biases found in the Southern Ocean are partially due to a positive shortwave radiation bias in the atmosphere model (Delworth et al. 2006). We also suspect that the shallow summer MLD bias (Fig. 3b) may in part be related to the lack of parameterized mixing associated with surface ocean gravity waves. This hypothesis is explored in the following.

1) EXP1: MS2000 PARAMETERIZATION

By implementing the MS2000 parameterization (Exp1), we anticipate deepening the summer mixed layer depth and thus affecting the SST warm bias in the Southern Ocean. Unfortunately, we see a larger SST bias globally in Exp1, with the SST root-mean-square error (RMSE) of 1.69°C in Exp1 versus 1.24°C in the control experiment (Fig. 2b). To better characterize the biases, we separate the globe into three zonal regions and calculate the RMSE for each region: Northern Hemisphere, $30^\circ\text{--}90^\circ\text{N}$;

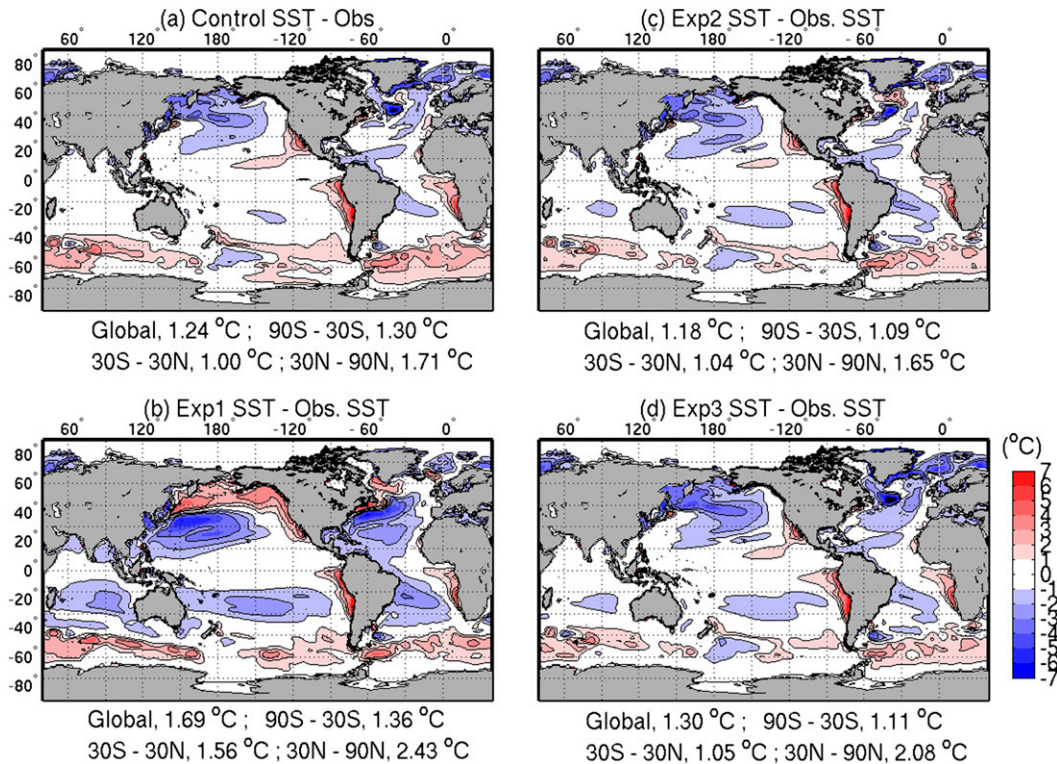


FIG. 2. Maps of errors in simulation of annual-mean SST ($^{\circ}\text{C}$) for the (a) control, (b) Exp1 (McWilliams and Sullivan 2000), (c) Exp2 (Smyth et al. 2002), and (d) Exp3 (Qiao et al. 2004) experiments. The errors are computed as model minus observations, where the observations are from the Reynolds SST data. The numbers below the panels give the SST RMSE for the globe, the Southern Hemisphere (90°S – 30°S), the equatorial region (30°S – 30°N), and the Northern Hemisphere (30°N – 90°N).

equator, 30°S – 30°N ; and Southern Hemisphere, 30° – 90°S . The largest SST error increase in Exp1 is found in the Northern Hemisphere with 0.72°C increase in RMSE, and the lowest increase is in the Southern Hemisphere with 0.06°C increase in RMSE.

Strong deepening of the winter MLD is found in Exp1 (Fig. 4c). The MLD becomes especially deeper than observations in the midlatitude storm track region. On the other hand, deepening of the summer MLD is negligible in both hemispheres (Fig. 3c), thus leading to minimal impact on the warm SST bias in the Southern Ocean. These results suggest that too much turbulent mixing is introduced by the MS2000 parameterization during winter, yet not enough turbulent mixing in the summer.

In the MS2000 parameterization, Langmuir turbulence impacts appear in the KPP scheme through the turbulent enhancement factor F_{L_t} [Eq. (1)]. When we multiply the enhancement factor to the turbulent velocity scale W , it also enters the calculation of BLD through the bulk Richardson number [Eq. (2)]. Thus, a larger turbulent velocity scale increases the BLD, whereas increases in stratification limit the deepening.

Since stratification is weaker during winter, enhancement of W will efficiently deepen the wintertime mixed layer. In contrast, the relatively strong stratification in summertime will restrain the deepening effect by the enhanced W .

2) EXP2: SMYTH ET AL. (2002) PARAMETERIZATION

Smyth et al. (2002) used the MS2000 scheme to study the upper-ocean response to a westerly wind burst in the equatorial Pacific. They found that the reduction in daytime warming is insufficient to reproduce their LES results quantitatively, while application of the MS2000 parameterization during nocturnal convection causes unrealistically rapid mixing throughout the mixed layer. Their finding is analogous to what we see in Exp1, where the MS2000 scheme generates too much mixing in winter and too little mixing in summer. Smyth et al. (2002) adjusted the MS2000 parameterization by adding the effect of stratification. Instead of using L_w in Eq. (1) as a constant, they changed it to a function of friction velocity u_* and the convective velocity scale w_* [Eq. (3)]. Through their modification, the turbulent enhancement

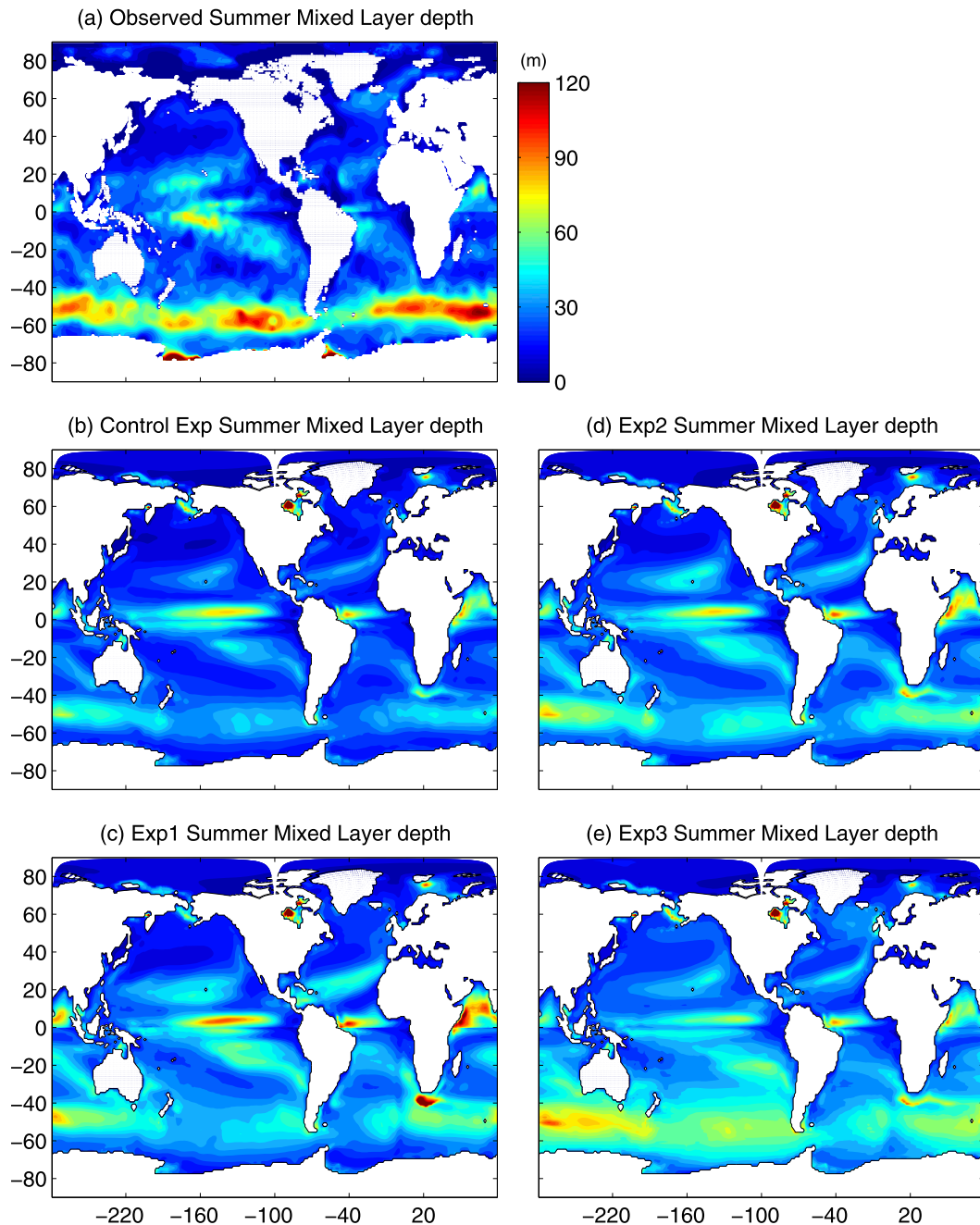


FIG. 3. Summer mean (JAS and JFM averages in the Northern and Southern Hemispheres, respectively) mixed layer depth from (a) observational estimates based on *World Ocean Atlas* data obtained from the National Oceanographic Data Center, and the (b) control, (c) Exp1, (d) Exp2, and (e) Exp3 experiments.

will be restrained under weak stratification conditions and magnified under strong stratification conditions.

By replacing the MS2000 parameterizations with the Smyth et al. (2002) parameterization in Exp2, we find that the SST bias in CM2M is improved globally (Fig. 2c) with a RMSE of 1.18°C (versus 1.24°C in the control). The major improvement is found in the Southern Ocean

with a reduction of 0.21°C in RMSE, while changes in the equatorial and Northern Hemisphere regions are small ($\pm 0.05^{\circ}\text{C}$). Reduction in the Southern Ocean SST warm bias is associated with a deeper summer MLD simulated in Exp2 (Fig. 3d) as compared to the control experiment (Fig. 3b). Notice that the Southern Ocean summer MLD in Exp2 is also deeper than Exp1,

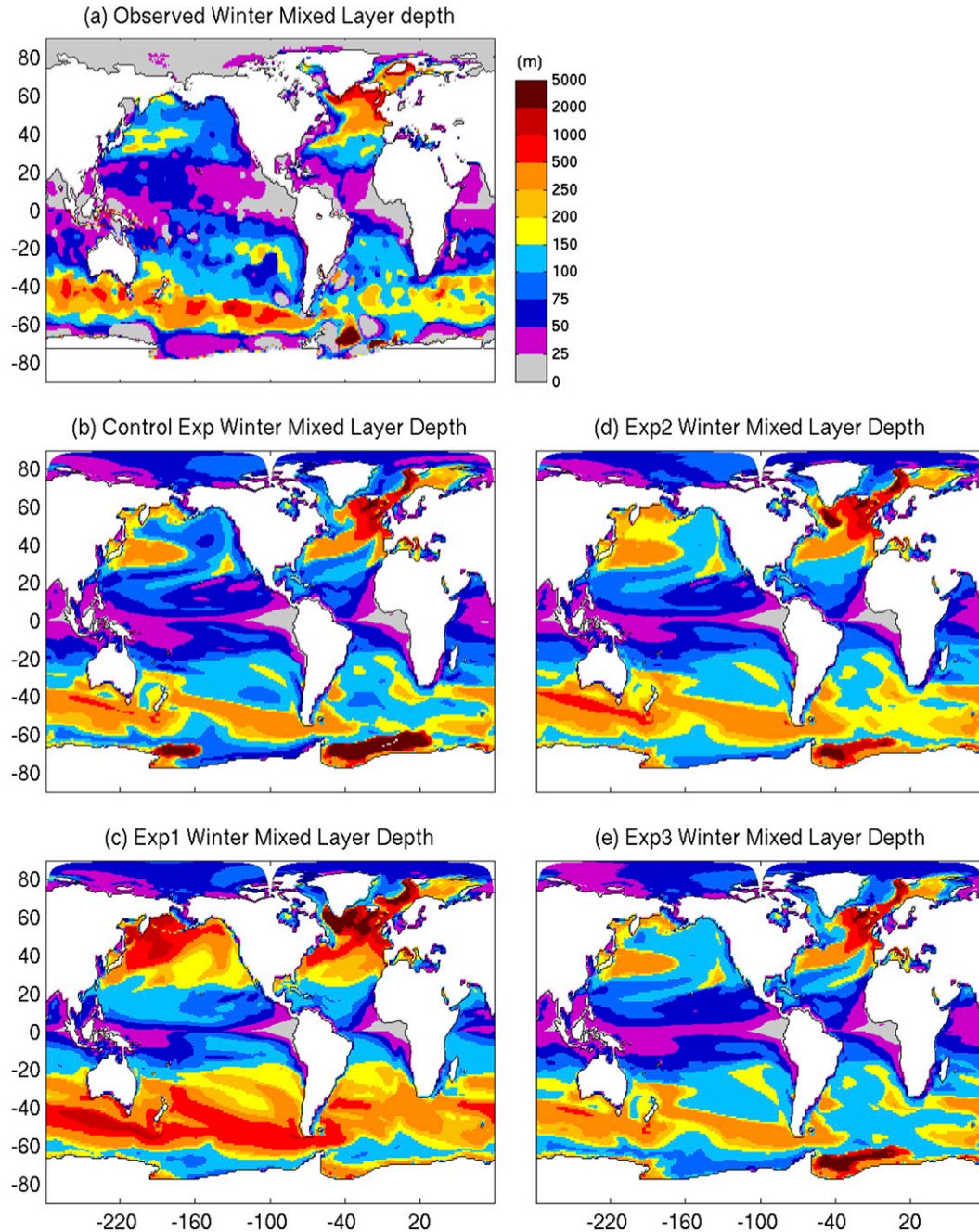


FIG. 4. As in Fig. 3, but for winter mean (JFM and JAS averages in the NH and SH, respectively).

indicating the improvement for our model by using the Smyth et al. (2002) parameterization versus MS2000.

The winter MLD in Exp2 (Fig. 4d) is also more reasonable compared with observations, including more mode and intermediate water formation in the Southern Ocean. Strong MLD deepening is observed in the Labrador Sea at comparable magnitude to the observations. And most interestingly, reduction of MLD is observed in the Weddell Sea and Ross Sea. The control simulation

with CM2M produces unrealistically strong convection in these regions and thus generates a very deep mixed layer of more than 2000 m. The CCSM4 model also shows an overly deep MLD in the Weddell Sea (Fig. 19 in Danabasoglu et al. 2012). Apparently, with the Langmuir turbulence parameterization, we are able to simulate more a realistic MLD in these regions of CM2M. We further discuss these features later in this section.

Despite the improvement particularly in the Southern Ocean, the simulated summer MLD remains shallower than observations, and the SST remains too warm. We suggest here three possible reasons for the remaining bias. One reason could be because of the relatively low resolution used in the atmosphere model, in which the strength of midlatitude storms are underestimated—the highest wind speed resolved by our model is 26 m s^{-1} , while the midlatitude storms very often have wind speeds exceeding 30 m s^{-1} (NCEP wind reanalysis; http://nomad3.ncep.noaa.gov/ncep_data). A low bias in wind speed leads in turn to a low wind stress and smaller-amplitude surface gravity waves. Thus, in the midlatitude region, we have a low bias in both the wind stress and turbulent enhancement from Stokes drift, which results in lower turbulent mixing and a warmer SST. A related problem could be that more wave characteristics need to be taken into consideration in parameterizing the mixing from Langmuir turbulence, besides just the Langmuir number and stratification that we used. In particular, we suggest that the misalignment between the Stokes drift and wind (Van Roekel et al. 2012) and the penetration depth of Stokes drift (Sullivan et al. 2012) may be important for more accurately parameterizing Langmuir turbulence effects (Harcourt and D'Asaro 2008; Webb and Fox-Kemper 2011; Raschle and Arduin 2013). Finally, the Southern Ocean SST warm bias may be dominated in our climate model by the positive shortwave radiation bias in the atmosphere model (Delworth et al. 2006), particularly in the summer.

3) EXP3: QIAO ET AL. (2004) PARAMETERIZATION

Qiao et al. (2004) used a different approach to parameterize the ocean surface gravity wave–induced turbulent mixing in the upper ocean. They proposed an adjustment to the vertical diffusivity and viscosity through integration of the wave spectrum. The physical idea is that the wave orbital velocity should enter the calculation of Reynolds stress. There is hence no clear separation between the Qiao et al. (2004) approach and the MS2000 and Smyth et al. (2002) approach, as the Stokes drift is the net residual of wave orbital motion. What makes Qiao et al. (2004) a very different approach is that their parameterized adjustment solely depends on the wave characteristics and does not depend on the depth of the boundary layer. Motivation for this feature of their scheme arises from noting that surface ocean gravity waves are not affected by ocean stratification.

Exp3 exhibits a reduction of 0.19°C in RMSE relative to the control experiment in the Southern Ocean using the Qiao et al. (2004) parameterization. However, the SST bias is increased elsewhere and globally (1.30°C ; Fig. 2d). Reduction in the SST warm bias in the Southern

Ocean is mainly due to deepening of the summer MLD (Fig. 3e) compared to the control (Fig. 3b). Notice the Southern Ocean summer MLD in Exp3 is deeper than both Exp1 and Exp2. However, in the winter, there is minimal improvement in the MLD (Fig. 4e). In particular, the MLD simulated in the Labrador Sea is even shallower than the control experiment. Furthermore, even though the MLD in the Ross Sea is improved, the improvement in the Weddell Sea is very limited.

This behavior of the Qiao et al. (2004) scheme is caused by the mixing length dependence on the wave decay scale [Eq. (5)]. Since the wave decay scale is comparable to or larger than the BLD during summer, the enhanced mixing coefficient B_v [Eq. (4)] can penetrate the entire boundary layer and in turn deepen the mixed layer. In contrast, during winter, the wave decay scale is typically shorter than the boundary layer depth and thus B_v has a negligible effect on deepening the mixed layer. Notably, Langmuir turbulence can penetrate far below the wave decay scale (Polton and Belcher 2007) and efficiently deepen the mixed layer during winter.

b. High latitudes with the Smyth et al. (2002) scheme

Overall, we consider that the Smyth et al. (2002) parameterization gives the most compelling improvements for our climate simulations with CM2M. Although these improvements are likely model dependent, it is instructive to more fully characterize some of the changes associated with this scheme as found in Exp2, with our focus on selected high-latitude regions. As we demonstrate below, it is the interactions between increased vertical mixing arising from the parameterized Langmuir turbulence and lateral transport, largely associated with parameterized mesoscale and submesoscale eddies, that lead to certain of the more intriguing, and sizable, impacts from this scheme.

1) LABRADOR SEA

We start by considering impacts in the Labrador Sea, where the control experiment is found to underestimate the winter MLD. By adding extra turbulent mixing through the Langmuir turbulent parameterization in Exp2, the winter MLD greatly deepened from the southern mouth of the Labrador Sea all the way to its northern end (Fig. 4d). In doing so, the simulation produces a Labrador Sea MLD that is closer to observations. In particular, the maximum MLD increased from less than 500 m to more than 2000 m at some locations.

The Labrador Sea is one of a few major open ocean deep convection sites in the World Ocean (Marshall and Schott 1999). The precondition in the Northern Hemisphere autumn (October–December) is a very important

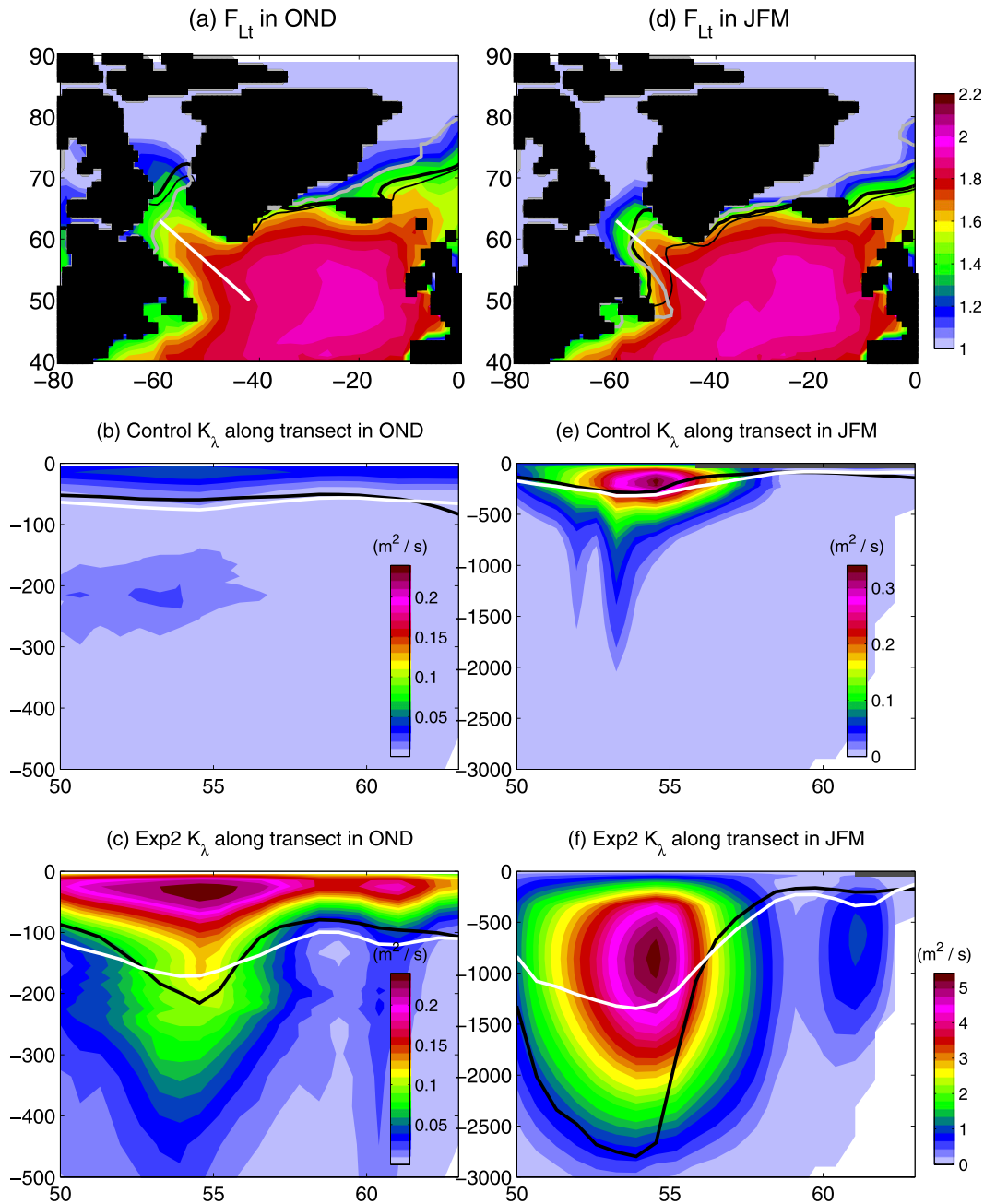


FIG. 5. Labrador Sea seasonal mean Langmuir turbulence enhancement factor F_{Lt} [determined by Eqs. (1) and (3)] in Exp2 for boreal (a) autumn and (d) winter. The thin black line, thick black line, and gray line indicate ice extent (ice concentration greater than 15%) for the control experiment, Exp2, and observations respectively. Also shown are the autumn mean vertical eddy diffusivity for (b) the control experiment and (c) Exp2 along the transect defined by the white line in (a) and the winter mean vertical eddy diffusivity for (e) the control experiment and (f) Exp2 along the transect defined by the white line in (d). In (b), (c), (e), and (f), the white (black) line represents boundary (mixed layer) depth, and the gray bar across the top indicates model ice extent.

factor for deep convection in the winter [January–March (JFM)]. The mean Langmuir turbulent enhancement factor F_{Lt} [Eqs. (1) and (3)] ranges from 1.4 at the northern end of the Labrador Sea to about 2 at the

mouth in the autumn (Fig. 5a). The sea ice extents are quite similar between the control experiment and Exp2, and more northward compared with the observations. To gain more understanding of the differences between

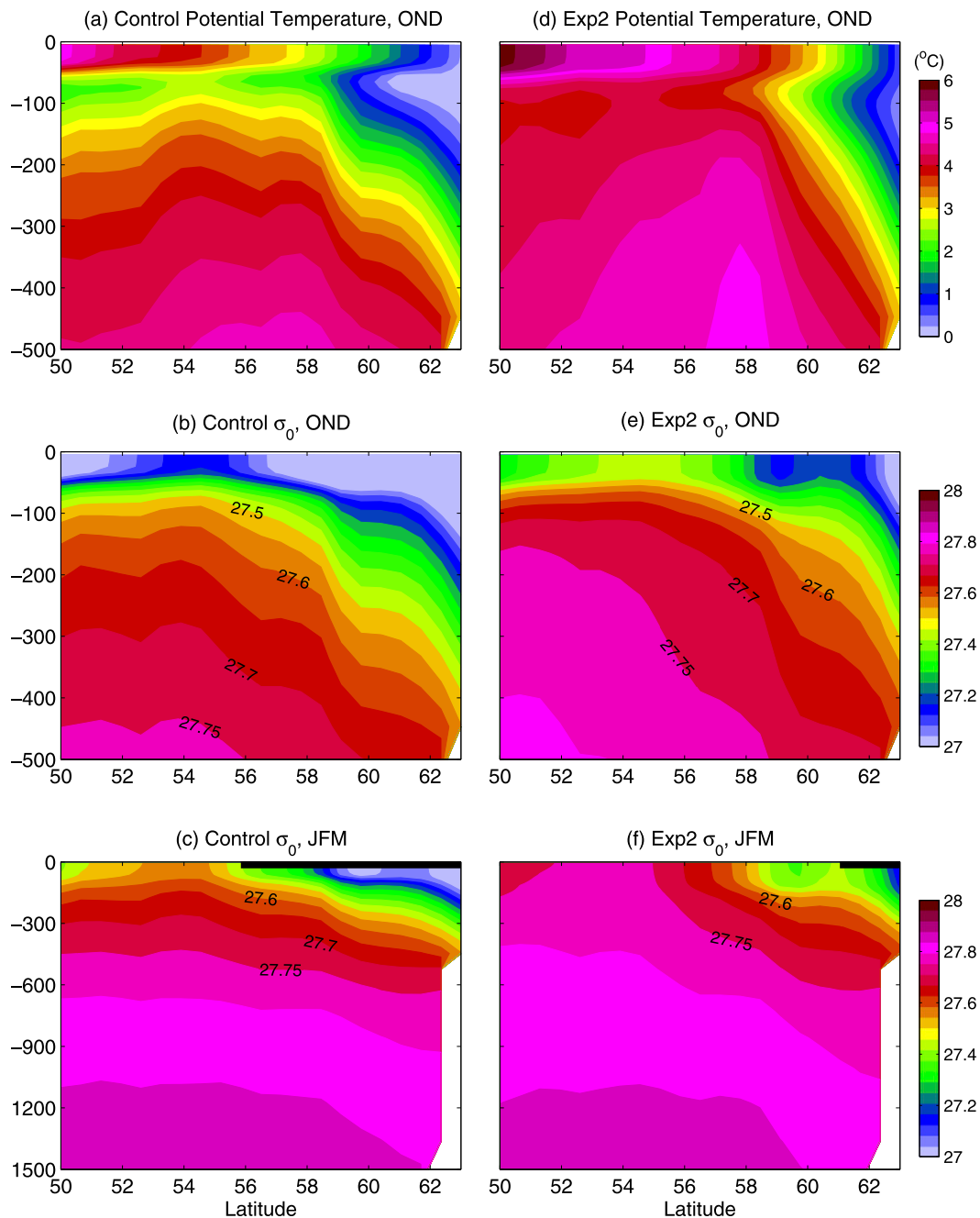


FIG. 6. Autumn mean (a) potential temperature, (b) potential density, and (c) winter mean potential density for the control experiment in the Labrador Sea. (d)–(f) As in (a)–(c), but for Exp2. In (c) and (f), the black bar across the top indicates model ice extent.

the control and Exp2, we examine the ocean state along a vertical transect of the Labrador Sea indicated by the white line in Fig. 5a.

The vertical eddy diffusivity (K_λ) in the control experiment is relatively small along the transect (Fig. 5b) during autumn, with shallow turbulent BLD and MLD (~ 50 – 60 m). This weak turbulent mixing cannot break

the strong stratification created in the summer due to surface warming. As a result, a thick cold layer lies between the warmer mixed layer and the thermocline (Fig. 6a). The strong temperature barrier creates a strong stratification in the surface water column (Fig. 6b), and limits how deep the convective mixing can penetrate in the winter. Note that we consider direct comparisons between the

control and Exp2 in Fig. 6, rather than differences. The reason is that we are concerned with the different stratification structures found in the two experiments (this comment also applies to Figs. 8 and 9, discussed later).

In Exp2, because of the strong turbulent mixing caused by the Smyth et al. (2002) Langmuir turbulence parameterization, K_λ is much stronger (Fig. 5c) than in the control, resulting in a doubling of the BLD and MLD. The strong turbulent mixing efficiently mixes warmer thermocline water into the surface layer from the thermocline below. The enhanced vertical mixing reduces stratification and increases the horizontal density gradient, which leads to enhanced lateral transport that mixes the surrounding North Atlantic Water into the Labrador Sea. In particular, to the southeast of the Labrador Sea, the northwestern loop of the North Atlantic Current transports warm water past the exit of the Labrador Sea. These warm waters are transported into the Labrador Sea by the enhanced lateral transport from the mesoscale and submesoscale eddy parameterization used in CM2M (see Dunne et al. 2012 for details). As a result, the surface layer warms, and the strong cold barrier is eliminated (Fig. 6d). Much weaker stratification is created at the surface and the weakly stratified warm interior water is brought closer to the surface (Fig. 6e). These effects provide a favorable precondition for deep convection to occur.

During the Northern Hemisphere winter (JFM), F_{Lr} is about the same magnitude as in the autumn. We find up to 2 times enhancement in the Labrador Sea in the ice-free regions (Fig. 5d). The ice extent in Exp2 (thick black line in Fig. 5d) is closer to observations, while the ice extends more southeast in the control experiment (far beyond the observations) and covers almost the entire Labrador Sea (thin black line in Fig. 5d). The sea ice is transported into the Labrador Sea either by the Labrador Current or through the Denmark Strait by the East Greenland Current. Since the surface temperature at the mouth of the Labrador Sea is much warmer in Exp2 (Fig. 6d), the sea ice transported toward the Labrador Sea by the East Greenland Current melts before entering the Labrador Sea.

Since the ice extends all the way to the mouth of the Labrador Sea in the control experiment, there is no interaction between the strong winter storms and the Labrador Seawater and, thus, no momentum flux into the ocean in the ice-covered region. Because of the strong surface stratification formed in autumn, buoyancy loss due to ice formation in this region is not strong enough to erode stratification and trigger deep convection. Therefore, the mixing activity beneath the sea ice is very low (i.e., the magnitude of K_λ is relatively small) (Fig. 5e). Mixing at the mouth of the Labrador Sea is

stronger compared to autumn because of strong winter storms. Weak deep convection penetrates to an approximate 2000-m depth. However, the deep convection is not strong enough to overcome the strong stratification built up in the autumn (Fig. 6c). As a result, the mixed layer deepening is limited to only 200–300 m, which is shallower than observations.

In Exp2, the sea ice extent is pushed into the northern end of the Labrador Sea, and the enhanced ocean mixing creates a weaker surface stratification in the autumn. When winter sets in, vigorous buoyancy loss due to surface cooling further erodes the near-surface stratification, thus exposing the weakly stratified water mass beneath. Unlike the control case, this region is ice free, thus exposing the ocean to strong winter storms. The enhanced mixing further reduces stratification. Then the subsequent cooling events initiate deep convection, in which a substantial part of the fluid column overturns and distributes the dense surface water in the vertical. We can see very large eddy diffusivity from the surface all the way to almost 3000-m depth (Fig. 5f). The largest eddy diffusivity is found between 500 and 1000 m, and is 10 times larger than the control experiment. As a result of the deep convection, the deep layer outcrops at the surface with very weak stratification beneath it (Fig. 6f). The BLD has deepened to approximately 1300 m, and the MLD has deepened to >2500 m. In contrast, for the control case, the stratification is largely maintained throughout winter.

The enhanced deep convection in the Labrador Sea in Exp2 leads to approximately 1.5 Sv ($1 \text{ Sv} \equiv 10^6 \text{ m}^3 \text{ s}^{-1}$) increase in Atlantic meridional overturning circulation (AMOC) compared with the control experiment (not shown). AMOC carries warm upper waters into northern latitudes and returns cold deep waters across the equator. Its large heat transport has a substantial influence on climate. Deep convection and bottom water formation in the Labrador Sea is an important factor influencing the strength of the AMOC (Delworth et al. 2008). In Exp2, the heat transport is increased by around 10%–20% in the middle–high latitudes of the Atlantic compared with the control experiment (not shown).

2) WEDDELL SEA

The control experiment produces unrealistically strong convection in the Ross Sea and Weddell Sea regions, and generates a very deep mixed layer of more than 2000 m in the winter (Fig. 4b). CCSM4 also shows a similarly deep mixed layer in the Weddell Sea (Fig. 19 in Danabasoglu et al. 2012). After applying the Smyth et al. (2002) Langmuir turbulence parameterization in Exp2, the MLD is reduced in both regions for our simulations (Fig. 4d) and becomes closer to observations

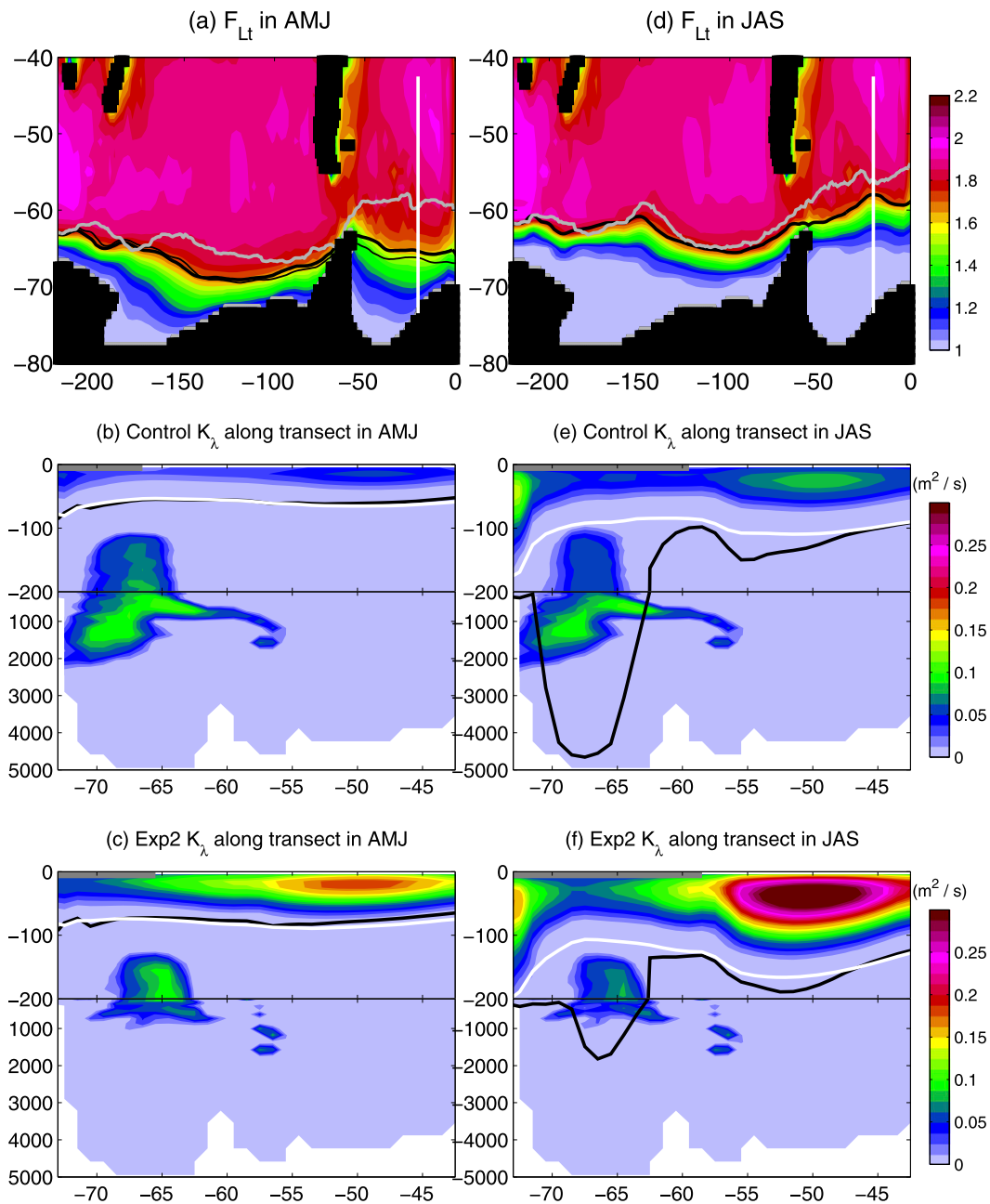


FIG. 7. As in Fig. 5, but for the Southern Ocean and austral autumn and winter.

(Fig. 4a). We were initially puzzled by this result, since we expected the enhanced mixing from parameterized Langmuir turbulence to deepen the mixed layer, as in the Labrador Sea. Subsequent analysis presented here exposed the importance of interactions between Langmuir mixing effects and parameterized mesoscale and submesoscale eddies.

The mean Langmuir turbulent enhancement factor, F_{Lt} , shows a similar magnitude in the Weddell and Ross Seas to those found in the Labrador Sea, for both the

austral autumn [April–June (AMJ)] and winter [July–September (JAS)] (Figs. 7a,d). The Southern Ocean sea ice extents in the control and Exp2 are very close to each other in the autumn, and virtually the same in the austral winter. The model sea ice growth is slower than observations for both seasons. To understand the mechanism for MLD reduction in the Ross Sea and Weddell Sea, we examine certain of the ocean responses along the Weddell Sea transect indicated by the white line in Figs. 7a and 7d.

In the Weddell Sea, the water column is well stratified with depth (Fig. 8b). The water to the south of 55°S is under sea ice during most of the year and thus much colder and saltier than water to the north. The salinity and temperature contrast are especially large in the top 100 m. Furthermore, the water is up to 1‰ saltier (Fig. 8a) and more than 6°C colder than the water north of 55°S (not shown). Deep convection is triggered by the thermobaric effect, which arises from the pressure dependence of the thermal expansion coefficient, with Gill (1973) and Killworth (1979) first recognizing the role of the thermobaric effect in their calculations/models of gravitational stability in the Weddell Sea.

Along the Weddell Sea transect, the distribution of K_λ does not change much with season (Fig. 7). Deep mixing occurs beneath the mixed layer year round for both the control experiment and Exp2. Ideal age (the age since water was last at the surface) is one way of looking at differences in ventilation. Figure 9 presents the ideal age of the two simulations averaged between model years 181 and 200. The control experiment shows strong deep ventilation (i.e., young ideal age) occurring to the south of 55°S, and penetrating all the way to more than 4000 m deep, while Exp2 only shows weak ventilation in the top 1000 m or so. One possible reason for enhanced ventilation in the control experiment could be that there is not enough lateral transport to draw stratified water into the ventilated region from the periphery and stabilize it after winter has passed.

The strong year-round deep ventilation in the control experiment creates a well-mixed deep layer beneath the boundary layer (Figs. 8c,d), which hardly varies with seasons (not shown). Deep ventilation is much weaker in Exp2 and unable to fully mix the deep layer like the control experiment, yet it reduces stratification in the water column (Fig. 8f) compared to the initial condition (Fig. 8b). Stratification of the water column beneath the boundary layer also hardly changes with season (not shown). Thus, it is the seasonal variation in the boundary layer that determines the MLD in both experiments.

As sea ice melts in the summer, the surface water becomes fresher and is warmed to about 4°C. The BLD and MLD become their shallowest during the year (~50 m), but the water beneath remains cold and thus creates a thermal barrier between the top layer and the ocean interior (not shown). In Exp2, the enhanced Langmuir turbulent mixing efficiently mixes more cold water into the boundary layer from below, which also increases the north–south lateral density gradient in the upper ocean. The increased density gradient leads to enhanced baroclinicity and an associated increased lateral transport through parameterized mesoscale and submesoscale eddies that mix fresher water from the

periphery north of the ice boundary into the boundary layer. These processes create a deeper, colder, and fresher boundary/mixed layer compared with the control experiment (not shown).

Sea ice starts to grow back in the autumn. The enhanced Langmuir turbulent mixing (Fig. 7c) together with enhanced lateral transport continues to mix more cold water from beneath and freshwater from the periphery into the boundary layer, and keeps the boundary layer deeper, colder, and fresher compared to the control experiment (not shown). When winter sets in, vigorous ice formation reduces the surface stratification by making the surface water colder and saltier. In Exp2, intense winter storms together with large surface waves create strong turbulent mixing in the water column (Fig. 7f), which has about 3 times the turbulent mixing of the control experiment (Fig. 7e). This strong turbulent mixing together with enhanced lateral transport efficiently mixes fresher water into the boundary layer from the periphery and keeps the surface stratification relatively strong (Figs. 8e,f). Because of the strong saline stratification built up in the surface layer, deep convection is greatly inhibited in Exp2 and is thus much weaker than the control experiment (Figs. 7e,f). Owing to the strong surface stratification and weak convection, stratification is maintained beneath the mixed layer in Exp2 (Fig. 8f).

For the control experiment, the turbulent boundary layer mixing and lateral transport are weaker compared to Exp2 in all seasons. As a result, the surface water is saltier and warmer in the summer. When sea ice starts to grow back in the autumn, the surface water becomes saltier because of ice formation. The weak turbulent mixing and lateral transport cannot mix enough fresher water from the periphery and the saline stratification becomes even weaker. When winter sets in, vigorous ice formation further reduces the surface saline stratification and triggers strong deep convection, while the weak turbulent mixing and lateral transport cannot mix enough fresher water from the periphery, in contrast to Exp2. Thus, the surface stratification is further reduced and matches with the interior water to produce a very deep mixed layer as diagnosed by the MLD criteria (potential density changes by 0.125 kg m^{-3} from its surface values). As a result, even though the BLD is deeper in Exp2, the MLD depth is much deeper in the control experiment.

3) ANTARCTIC CIRCUMPOLAR CURRENT

Stratification changes in the Weddell Sea give rise to pressure gradient changes across the Drake Passage and impact transport through the Antarctic Circumpolar Current (ACC). The enhanced turbulent mixing in Exp2

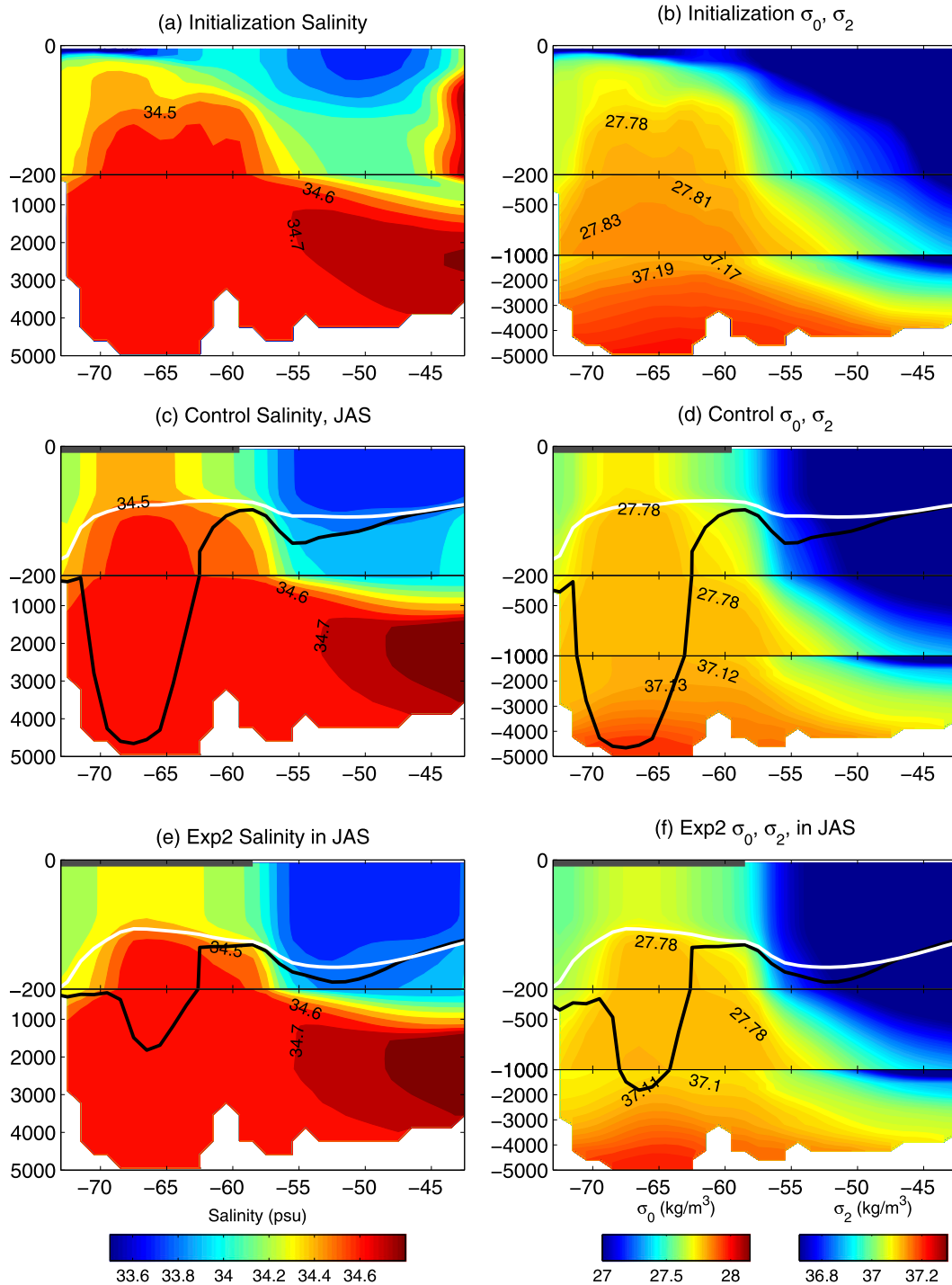


FIG. 8. Weddell Sea initial condition of (a) salinity and (b) potential density along the vertical transect defined in Fig. 7a. Also shown are winter mean (c),(e) salinity and (d),(f) potential density for the control experiment and Exp2, respectively. In (c)–(f), the white (black) line represents boundary (mixed) layer depth, and the gray bar across the top indicates model ice extent.

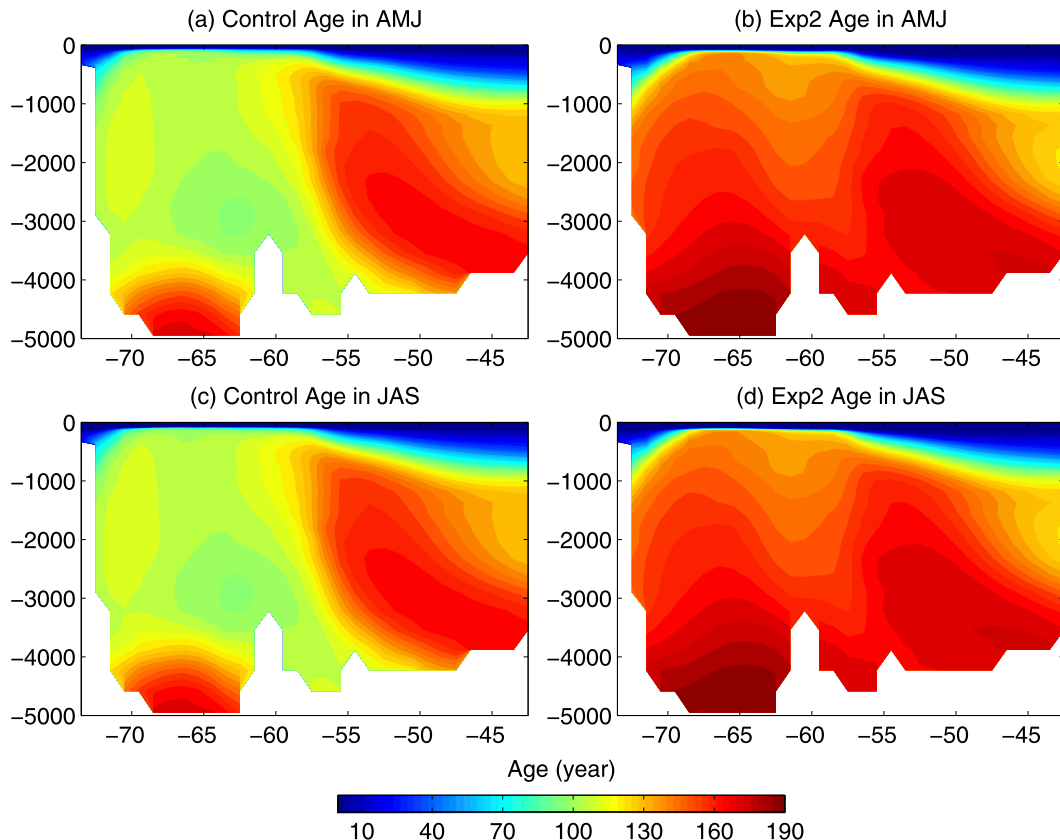


FIG. 9. Autumn 20-yr mean (model years 181–200) age for (a) the control experiment and (b) Exp2 along the Weddell Sea transect defined in Fig. 7a. Winter 20-yr mean age for (c) the control experiment and (d) Exp2 along the Weddell Sea transect.

helps to maintain stratification in the Weddell Sea, which leads to a reduction of the pressure gradient across the Drake Passage and decrease of ACC transport (Fig. 10a). We are particularly interested here in the sharp increase of ACC transport in Exp2 between model years 449 and 462 (thick red line in Fig. 10a). We note that no analogous event is seen in the 500-yr control simulation. We speculate at the end of section 4 why this polynya-like event did not occur in the control.

To help understand the cause for the polynya-like event in Exp2, we calculated the southern annular mode (SAM) index for Exp2 from model years 401 to 500. Variations in the SAM arise from climate variability in the Southern Hemisphere, with the SAM index providing a useful measure of the variability. Meredith et al. (2004) found evidence that the SAM forces interannual variability of the ACC transport through Drake Passage. We use the Gong and Wang (1999) method to calculate the SAM index in our study, which uses the difference between normalized zonal mean sea level pressure between 40° and 65°S.

During the austral autumn, we find continuously strong negative SAM from around model years 440–462

with weak positive SAM present every couple of years during this period (Fig. 10b). In the troposphere, the SAM is characterized by nearly zonally symmetric, north–south variability in the latitude of the midlatitude jet and its associated wave fluxes of heat and momentum. The negative phase of the SAM is marked by northward displacements of the jet and thus weakening of the prevailing atmospheric eastward flow near approximately 60°S (Thompson and Wallace 2000). In the Weddell Sea, sea ice is formed in the southern part and transported northward and then eastward by the Weddell Sea Gyre. Weaker westerlies between 50° and 70°S decrease the wind stress curl, and so slow down the Weddell Sea Gyre and shift it southward (Jullion et al. 2010). After continuously having the negative phase of SAM for about 5 yr (by model year 445), the Weddell Sea Gyre is noticeably slowed down (not shown), which leads to a decrease of the northward advection of sea ice and reduction in sea ice concentration in the Weddell Sea (Fig. 10c).

When winter sets in, the ice-free region is exposed to the strong winter storms. Enhanced turbulent mixing

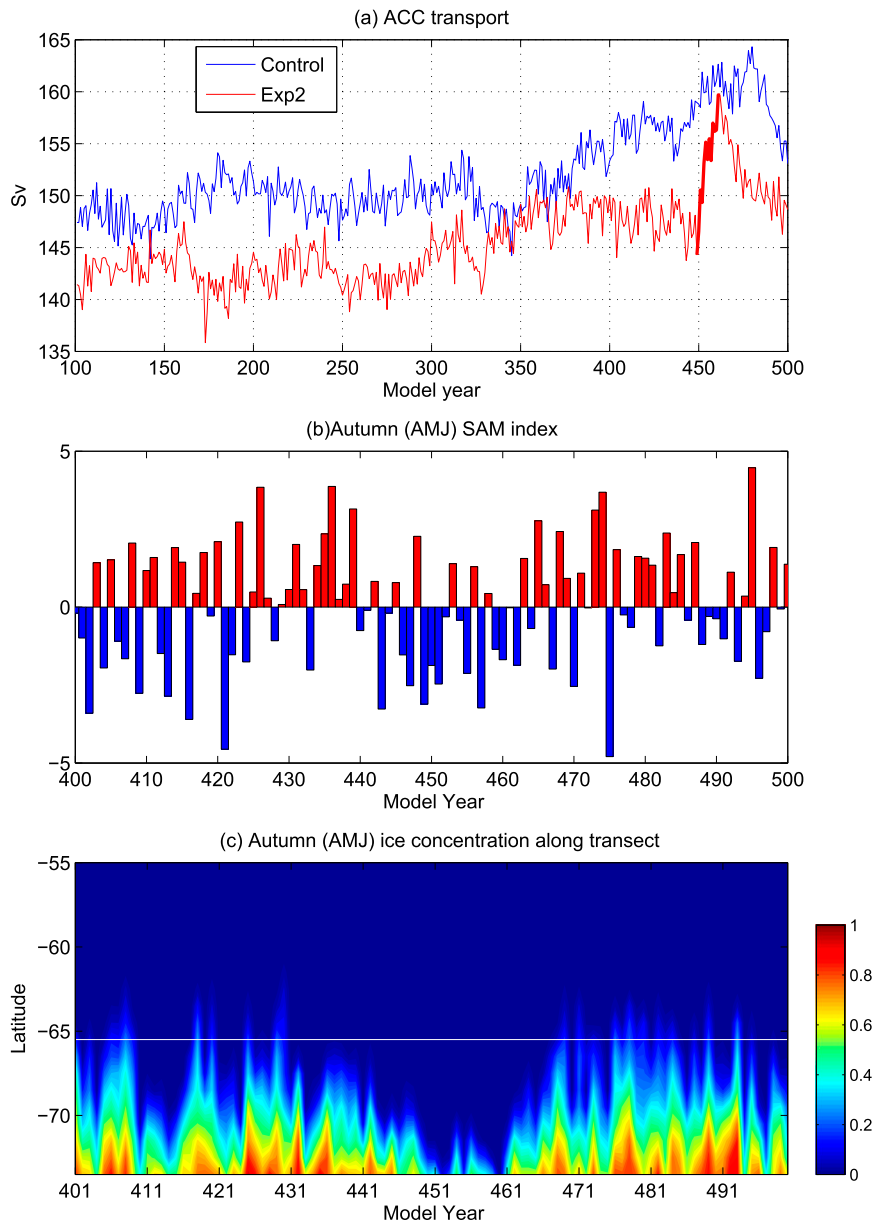


FIG. 10. (a) ACC transport across the Drake Passage from model years 101 to 500 for the control experiment (blue) and Exp2 (red). Exp2 autumn (AMJ) (b) SAM index from model years 401 to 500, and (c) ice concentration along the horizontal transect defined in Fig. 7d from model years 401 to 500.

entrains warm water into the surface layer from the thermocline below it, and further reduces the possibility for ice growth in the region (Fig. 11a). Vigorous buoyancy loss resulting from surface cooling together with enhanced turbulent mixing by the strong winter storms gradually erode the near-surface stratification away year by year, and exposes the weakly stratified water mass beneath.

Around model year 450 (about 5 yr after the sea ice extent retreated southward), the surface stratification

becomes weak enough for surface cooling to trigger strong deep convection. A large part of the fluid column overturns and distributes the warm thermocline water in the vertical (Fig. 11c). We can see very large eddy diffusivity from the surface all the way to almost 5000-m depth (Fig. 11b). As a result, the ocean releases a huge amount of heat to the atmosphere, and the whole water column becomes uniform in temperature (Fig. 11c).

Because of the warm sea surface, ice melts in the region with deep convection throughout the water

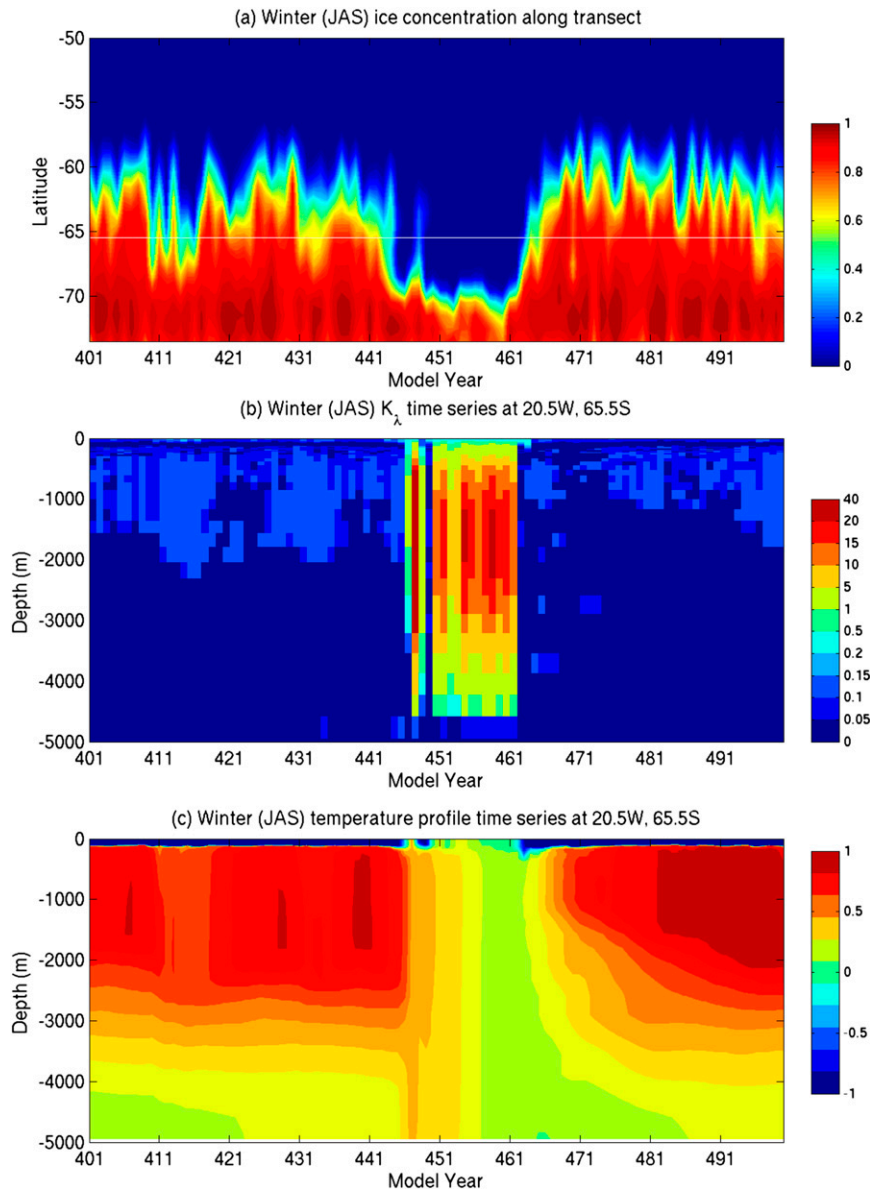


FIG. 11. Exp2 austral winter (JAS) (a) ice concentration along the horizontal transect defined in Fig. 7d from model years 401 to 500. (b) Vertical eddy diffusivity and (c) temperature profile at 65.5°S, 20.5°W from model years 401 to 500.

column, and the transport of ACC increases dramatically (Fig. 10a). The ACC transport decreases rapidly during the continuously positive phases of SAM after model year 462.

4. Summary and discussion

In this study, the effect on simulated global climate from parameterized mixing associated with surface ocean gravity waves is assessed through modification to the K -profile ocean boundary layer parameterization

(Large et al. 1994). Our tool for this assessment is a fully coupled atmosphere–ocean–wave global climate model. In this coupled system, WAVEWATCH III, the operational wave model developed and used at NCEP, is incorporated into the GFDL climate model CM2M. Two Langmuir turbulence parameterizations and one nonbreaking wave parameterization are evaluated using the fully coupled system.

For our simulations, the McWilliams and Sullivan (2000) Langmuir turbulence parameterization produced too much turbulent mixing during winter, yet not

enough turbulent mixing in the summer. In their scheme the Langmuir turbulence effect is brought into KPP through an enhancement factor F_{Lt} that multiplies the turbulent velocity scale W . Thus, F_{Lt} also enters the calculation of boundary layer depth (BLD) through the bulk Richardson number. A larger W , as occurs in regions of active Langmuir turbulence, works to increase the BLD, while stratification works to limit the deepening. Since the stratification is weak during winter, enhancement of W deepens the winter mixed layer. In contrast, during summer the stronger stratification restrains the deepening effect from their scheme.

The Smyth et al. (2002) parameterization introduces stratification effects to the McWilliams and Sullivan (2000) parameterization so that the turbulent enhancement is restrained under weak stratification conditions and magnified under strong stratification conditions. By using the Smyth et al. (2002) parameterization, our simulated SST bias is improved globally compared with the original CM2M results (the global root-mean-square error is improved by 6%). The largest improvement is found in the Southern Ocean and is associated with a deeper summer MLD (the SST root-mean-square error is improved in this region by 15%), although the model simulated summer mixed layer is still shallower than observations.

Although the Smyth et al. (2002) scheme reduced the Southern Ocean biases in SST and MLD, we suggest that other biases or limitations may need to be addressed in our simulations to further reduce the biases. One important reason could be that because of inadequate resolution used in the atmosphere model, the intensity of midlatitude storms is underestimated, which in turn leads to smaller (wave height and wavelength) surface ocean waves. Thus, the midlatitudes have a low bias in both the wind stress and turbulent enhancement due to Stokes drift, which in turn results in lower turbulent mixing and warmer SST. This result points to the intimate relation between parameterized surface ocean gravity wave mixing and the atmospheric simulation. Relatedly, we could be encountering limitations of the Langmuir mixing parameterizations considered here, in which more wave characteristics may need to be taken into consideration, besides the Langmuir number and stratification. Particular features include the misalignment between the Stokes drift and wind (Van Roekel et al. 2012) and the penetration depth of Stokes drift (Sullivan et al. 2012). Another possibility for the remaining shallow MLD bias may be related to the positive shortwave radiation bias in the atmosphere model in the Southern Ocean (Delworth et al. 2006).

Qiao et al. (2004) argue that the wave orbital velocity should enter the calculation of Reynolds stress. They

proposed an adjustment to the vertical diffusivity and viscosity through integration of the wave spectrum. Their parameterized adjustment depends solely on the wave characteristics and, in particular, is independent of the boundary layer thickness. Their parameterization provides the strongest summer mixed layer deepening in the Southern Ocean among the three experiments, but the effects are very weak elsewhere and during the winter. This behavior of the Qiao et al. (2004) scheme is caused by the mixing length dependence on the wave decay scale [Eq. (5)]. Since the wave decay scale is comparable to or larger than the MLD during summer, the mixing coefficient B_v [Eq. (4)] can penetrate the entire summer mixed layer and deepen it. During winter, the wave decay scale is much shorter than the MLD and thus the enhanced mixing coefficient B_v has negligible effect on deepening the winter mixed layer.

In contrast, Langmuir turbulence can penetrate far below the wave decay scale (Polton and Belcher 2007) and efficiently deepen the winter mixed layer. However, the current parameterizations used in this study limits the Langmuir turbulence to within the boundary layer, and neglects the fact that the wave decay scale could be deeper than the BLD in the summertime and the downwelling jet can penetrate even deeper, as demonstrated in Polton and Belcher (2007). Thus, we believe a new parameterization is needed with better representation of the depth penetration of Langmuir turbulence. Note that since the Stokes drift is the net residual of wave orbital motion, there is no clear separation between the Qiao et al. (2004) approach and the MS2000 and Smyth et al. (2002) approach, so these schemes should not be applied together.

With the Smyth et al. (2002) parameterization, strong mixed layer deepening is observed in the Labrador Sea bringing the MLD closer to observations in our simulations. Surprisingly, reduction of MLD is found in the Weddell Sea and Ross Sea, also bringing our simulations closer to observations. Through analyzing the model behavior at the Labrador Sea and the Weddell Sea, we found that even though the Langmuir turbulence parameterization is applied to enhance the vertical mixing in the KPP scheme, the coupling with enhanced lateral transport is the key for improving mixed layer simulations.

Our results suggest that the enhanced vertical mixing in the boundary layer creates lateral variations in the temperature and salinity fields, which lead to enhanced lateral transport. Through enhanced lateral transport, warm water is brought into the Labrador Sea from the periphery. The warm water melts the ice and reduces surface stratification through enhanced vertical mixing, and creates an ideal condition for deep convection in the winter. In the Weddell Sea, enhanced lateral transport

brings saltier water from the periphery and increases surface stratification through enhanced vertical mixing, which inhibits deep convection and shoals the mixed layer.

We also found the occurrence of a polynya-like event in the Weddell Sea is correlated with variations in the southern annular mode (SAM). Continuous negative phases of SAM decrease westerlies between 50° and 70°S, slow down the Weddell Sea Gyre, and create a polynya in the Weddell Sea. The onset of the polynya lags the onset of persistent negative SAM for approximately 5 yr. During the polynya, deep convection homogenizes the water column and releases huge amounts of heat to the atmosphere. Such stratification changes in the Weddell Sea result in an increase in the pressure gradient across the Drake Passage and increases the Antarctic Circumpolar Current (ACC) transport. The ACC transport starts to increase at the onset of the deep ventilation, which lags the onset of the polynya by roughly 5 yr. That is, the ACC transport starts to increase 10 yr after the onset of the persistent negative SAM.

There is no polynya-like event found in the control run. We speculate that the reduced convection in the Weddell Sea in Exp2 with the Smyth et al. (2002) Langmuir turbulence parameterization allows for more long-term storage of heat at depth. This result presents yet another surprising way that upper-ocean mixing in the high latitudes through ocean surface gravity waves may play a nontrivial role in climate fluctuations.

5. Concluding remarks

a. Climate simulations and upper-ocean mixing processes

There are several physical processes that affect upper-ocean mixing and stirring besides Langmuir turbulence. Examples include mesoscale eddies, submesoscale eddies, convection, and near-inertial waves. Interactions among these processes are complex and may lead to unexpected behavior. Our study exemplifies such unexpected behavior, in which the mixed layer depth is greatly reduced (and made more realistic) in the Weddell and Ross Seas in a simulation with parameterized Langmuir turbulence, relative to a control simulation that did not have parameterized Langmuir turbulence. We additionally found polynya-like events in the Weddell Sea with parameterized Langmuir turbulence, whereas they are absent from the control simulation.

We do not presume these model results provide the final word on interactions between wave-induced mixing and other transport processes of relevance to climate. We nonetheless suggest the results point to the importance of gauging the impact from ocean surface gravity

wave mixing, and other mixing processes, within the context of realistic climate simulations. We are particularly intrigued by the sizable and complex interactions between wave-induced vertical mixing and high-latitude processes associated with sea ice and mesoscale and submesoscale eddy transport. These results suggest fruitful avenues for process-based studies with ocean wave-induced mixing within refined resolution simulations where the mesoscale and submesoscale eddy processes are explicitly resolved. One aim would be to provide physical insights important for identifying robust behavior in support of accurate parameterizations used in coarse climate simulations.

Our focus on the impacts of surface ocean gravity wave-induced mixing is reflective of an analogous study by Jochum et al. (2013), who considered near-inertial wave (NIW)-induced mixing. They found that parameterized NIW mixing can deepen the MLD by up to 30%, and deepening of the tropical mixed layer by NIWs can lead to a change in tropical SST and precipitation. Since a diurnal cycle is included in all surface fluxes in our experiments, including wind stress, our simulations presumably maintain a nontrivial degree of inertial energy to the degree provided by the atmospheric model. Even though the spatial distribution and magnitude of NIWs in the midlatitude storm region is very similar to Stokes drift, the global patterns between these two wave fields are very different. The Stokes drift is very weak in the equatorial region where NIWs appear to be the strongest.

b. Why we need a surface wave model to parameterize surface wave-induced mixing

Given computational limitations, current large-scale climate models are incapable of explicitly resolving certain of the complex physical processes involved in upper-ocean mixing. Since upper-ocean processes are crucial for determining atmosphere-ocean fluxes in climate models, the development of upper-ocean mixing parameterization is an area that deserves extensive research efforts. In particular, the different behavior of the two Langmuir turbulence parameterization schemes used in this study suggest that more physical pieces may be needed in the parameterizations, besides Stokes drift. Further tuning of the coefficients in the Smyth et al. (2002) parameterization did not give better results (not shown), which also emphasizes the need for better understanding of the physics of Langmuir turbulence.

Many wave-dependent processes are currently parameterized within coupled ocean-atmosphere general circulation models using wind-dependent parameterizations (Cavaleri et al. 2012). This is a valid simplification if winds and waves are in equilibrium. However, Fan et al. (2014) shows this local equilibrium assumption

is not respected over the majority of the ocean, with swell dominating the global wave field. To demonstrate this effect here, we compared the wind speed parameterized surface Stokes drift with wave model generated Stokes drift in [appendix B](#). Our results suggest that the wind-dependent parameterized Stokes drift is not a good representation of the wave model generated Stokes drift, largely attributable to the lack of a local equilibrium between wind and waves. This result provides a strong reason to use a dynamic surface wave model to compute parameterized wave-induced mixing in the coupled climate models.

Even though there is a growing appreciation of the dynamical importance of surface ocean waves in upper-ocean mixing, concerns arise on the computational cost of the dynamic surface wave model. In the experiments presented in this paper, the wave model is run at a grid resolution corresponding to the atmospheric model, which is coarser than the ocean model. Following [Fan et al. \(2012\)](#), we suggest it more critical for climate applications to refine the frequency and wavenumber representation of the surface waves rather than to employ refined horizontal grid resolution. In our model configuration, the wave model is less expensive than the atmospheric model at the same resolution, and cheaper than the ocean model at finer resolution.

c. Potential importance of surface waves for Arctic climate change studies

We close this paper by offering a speculation for one area where ocean surface gravity wave mixing may play a very significant role in climate change. Namely, as Arctic sea ice melts, the upper ocean is exposed to mixing by ocean surface waves that were previously absent. Such mixing may in turn erode the Arctic pycnocline separating the upper Arctic Ocean from the warm Atlantic waters at intermediate depths. In particular, during the boreal autumn, when the midlatitude storms become strong and are accompanied by large ocean surface gravity waves, the sea ice area in the Arctic Ocean also reaches its minimum. Strong surface gravity wave-induced turbulent ocean mixing can reduce the surface stratification and provide the necessary precondition for convection in the Arctic Ocean. In so doing, this enhanced ventilation could release heat from the deep Arctic, thus accelerating sea ice melt. As [Rainville et al. \(2011\)](#) have pointed out, with an increasing fraction of the Arctic Ocean becoming ice-free in summer and autumn, there is a crucial need for a better understanding of the impact of direct wind forcing on the Arctic Ocean. We suggest that this role for surface ocean gravity waves may be critical for projecting Arctic climate change over the coming decades.

Acknowledgments. The authors would like to express their appreciation to Drs. Thomas Delworth, Shiann-Jian Lin, and Michael Winton for their enthusiastic support of this project. We also thank Drs. Alistair Adcroft, John Dunne, Baylor Fox-Kemper, Matthew Harrison, Bill Large, Sonya Legg, Ronald Stouffer, Erick Rogers, and the anonymous reviewers for very helpful comments and suggestions. We thank Dr. Zhi Liang for help developing the coupled system used in this study. The assistance of the GFDL computational and administrative support services staff is furthermore greatly appreciated.

APPENDIX A

Physical Components of CM2M

The physical components of CM2M include four models: atmosphere, land, sea ice, and ocean.

The GFDL Atmospheric Model, version 2 (AM2), uses a finite volume dynamic core and has a grid spacing of 2.5° longitude by 2° latitude and 24 vertical levels. The model contains a suite of model physics including cloud prediction and boundary layer schemes, and diurnally varying solar insolation. The radiation code allows for explicit treatment of numerous radiatively important trace gases (including tropospheric and stratospheric ozone, halocarbons, etc.), a variety of natural and anthropogenic aerosols (including black carbon, organic carbon, tropospheric sulfate aerosols, and volcanic aerosols), and dust particles. Aerosols in the model do not interact with the cloud scheme, so that indirect aerosol effects on climate are not considered. Further details and references can be found in [Delworth et al. \(2006\)](#).

The ocean component of CM2M employs the MOM, version 4.1 (MOM4p1), code of [Griffies \(2009\)](#) configured with the same grid and bathymetry as the CM2.1 ocean component ([Gnanadesikan et al. 2006](#); [Griffies et al. 2005](#)). The new features in MOM4p1 are detailed in [Dunne et al. \(2012\)](#). MOM4p1 uses a tripolar grid with 1° grid spacing in latitude and longitude poleward of 30°N and 30°S. The meridional resolution becomes progressively finer equatorward and reaches about 1/3° at the equator. The poles are set over Eurasia, North America, and Antarctica to avoid polar filtering over the Arctic. The model has 50 vertical levels, including 22 levels with 10-m thickness each in the top 220 m.

The Land Model, version 3 (LM3), is utilized in CM2M. LM3 is a model for land water, energy, and carbon balance. In comparison to its predecessor (see [Milly and Shmakin 2002](#)), LM3 includes more comprehensive models of snowpack, soil water, frozen soil and water, groundwater discharge to streams, and

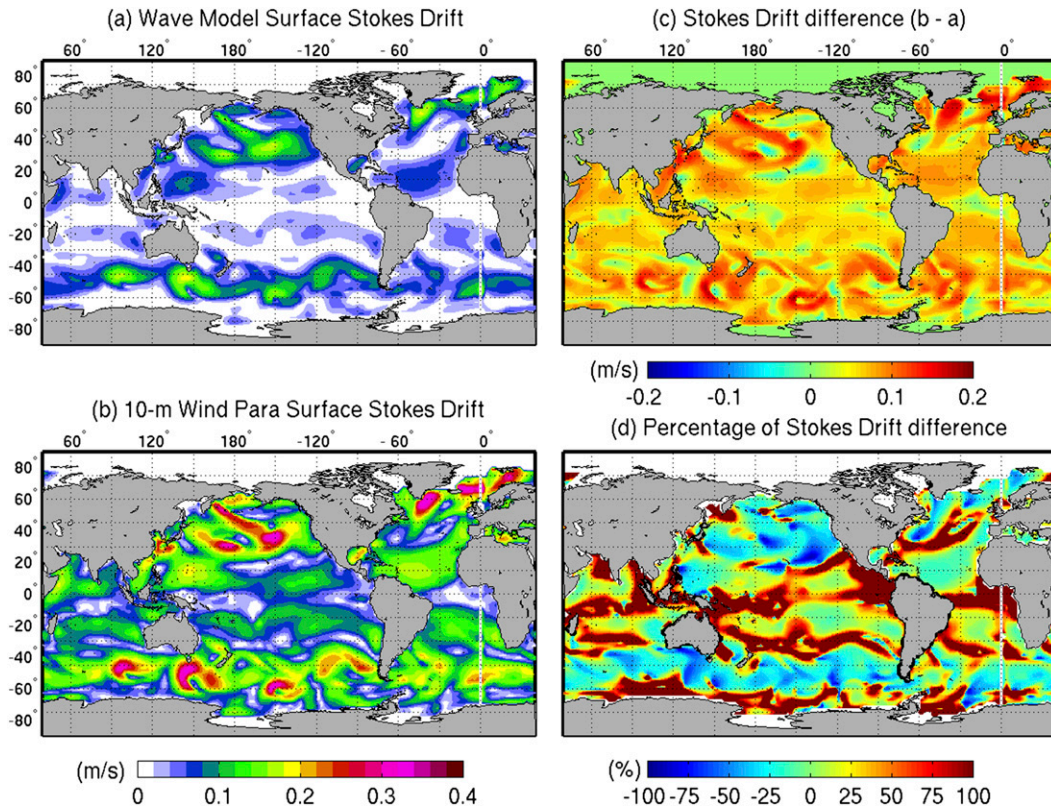


FIG. B1. Surface Stokes drift from the (a) wave model and (b) Li and Garrett (1993) parameterization, (c) their differences [(b) minus (a)], and (d) the percentage of differences between the adjusted surface Stokes drift from the Li and Garrett parameterization and the wave model simulated surface Stokes drift relative to the model-simulated surface Stokes drift. Note that (a) and (b) share the same color bar.

finite-velocity horizontal transport of runoff via rivers to the ocean. LM3 uses the same grid configuration as the atmospheric model.

The sea ice model is a dynamical model with three vertical layers and five ice thickness categories. The model uses the elastic viscous plastic rheology to calculate ice internal stresses, and a modified Semtner three-layer scheme for thermodynamics (Winton 2000). Further details are provided by Delworth et al. (2006).

APPENDIX B

Surface Stokes Drift Parameterization

Li and Garrett (1993) proposed a surface Stokes drift, $U_s(0)$ parameterization as a function of the 10-m wind speed U_w .

$$U_s(0) = 0.016U_w. \quad (\text{B1})$$

To test this parameterization, we randomly take a snapshot of 10-m wind speed from our coupled model

during the boreal winter and parameterize $U_s(0)$ using Eq. (B1) as shown in Fig. B1b. The corresponding surface Stokes drift calculated from our coupled model is given in Fig. B1a, and the difference is given in Fig. B1c. The parameterized Stokes drift is larger than the model generated Stokes drift almost everywhere in the global ocean, and the differences are more pronounced in the midlatitude storm region.

To reduce differences between the parameterized and model simulated Stokes drift, we adjusted the parameter in Eq. (B1) from 0.016 to 0.0067 so that the root-mean-square error between the parameterized and model-simulated surface Stokes drift is at a minimum. The percentage differences (the difference between the adjusted parameterized Stokes drift and the model simulated values divided by the model simulated values) are given in Fig. B1d. We can see both overestimates and underestimates of the midlatitude region and overestimates in the tropical region. The overestimations are more than 100% in a large area of the global ocean, and the underestimations are up to 100% at many places as well. We also tried to adjust the parameterized surface

Stokes drift based on matching its mean value, maximum value, or standard deviation with the model-simulated surface Stokes drift, but none of our attempts reduced the differences.

Although our tuning exercise for the local wind-dependent Stokes drift parameterization is not exhaustive, we believe these tests are sufficient to conclude that the wind-dependent parameterized Stokes drift is not a good representation of the wave model generated Stokes drift. The key point is that winds and waves are not in local equilibrium over the majority of the ocean, with swell dominating the global wave field (Fan et al. 2014).

REFERENCES

- Babanin, A. V., A. Ganopolski, and W. R. C. Phillips, 2009: Wave-induced upper-ocean mixing in a climate model of intermediate complexity. *Ocean Modell.*, **29**, 189–197, doi:10.1016/j.ocemod.2009.04.003.
- Bates, S. C., B. Fox-Kemper, S. R. Jayne, W. G. Large, S. Stevenson, and S. G. Yeager, 2012: Mean biases, variability, and trends in air–sea fluxes and sea surface temperature in the CCSM4. *J. Climate*, **25**, 7781–7801, doi:10.1175/JCLI-D-11-00442.1.
- Belcher, S. E., and Coauthors, 2012: A global perspective on Langmuir turbulence in the ocean surface boundary layer. *Geophys. Res. Lett.*, **49**, L18605, doi:10.1029/2012GL052932.
- Booij, N., R. C. Ris, and L. H. Holthuijsen, 1999: A third-generation wave model for coastal regions 1. Model description and validation. *J. Geophys. Res.*, **104**, 7649–7666, doi:10.1029/98JC02622.
- Cavaleri, L., B. Fox-Kemper, and M. Hemer, 2012: Wind waves in the coupled climate system. *Bull. Amer. Meteor. Soc.*, **93**, 1651–1661, doi:10.1175/BAMS-D-11-00170.1.
- Craik, A. D. D., and S. Leibovich, 1976: A rational model for Langmuir circulations. *J. Fluid Mech.*, **73**, 401–426, doi:10.1017/S0022112076001420.
- Danabasoglu, G., S. C. Bates, B. P. Briegleb, S. R. Jayne, M. Jochum, W. G. Large, S. Peacock, and S. G. Yeager, 2012: The CCSM4 ocean component. *J. Climate*, **25**, 1361–1389, doi:10.1175/JCLI-D-11-00091.1.
- Delworth, T., and Coauthors, 2006: GFDL’s CM2 global coupled climate models. Part I: Formulation and simulation characteristics. *J. Climate*, **19**, 643–674, doi:10.1175/JCLI3629.1.
- , and Coauthors, 2008: The potential for abrupt change in the Atlantic meridional overturning circulation. *Abrupt Climate Change: Final Report, Synthesis and Assessment Product 3.4*, DIANE Publishing, 258–359.
- Dunne, J. P., and Coauthors, 2012: GFDL’s ESM2 global coupled climate–carbon earth system models. Part I: Physical formulation and baseline simulation characteristics. *J. Climate*, **25**, 6646–6665, doi:10.1175/JCLI-D-11-00560.1.
- , and Coauthors, 2013: GFDL’s ESM2 global coupled climate–carbon Earth system models. Part II: Carbon system formulation and baseline simulation characteristics. *J. Climate*, **26**, 2247–2267, doi:10.1175/JCLI-D-12-00150.1.
- Fairall, C. W., E. F. Bradley, J. E. Hare, A. A. Grachev, and J. B. Edson, 2003: Bulk parameterization of air–sea fluxes: Updates and verification for the COARE algorithm. *J. Climate*, **16**, 571–591, doi:10.1175/1520-0442(2003)016<0571:BPOASF>2.0.CO;2.
- , M. L. Banner, W. L. Peirson, W. Asher, and R. P. Morison, 2009: Investigation of the physical scaling of sea spray spume droplet production. *J. Geophys. Res.*, **114**, C10001, doi:10.1029/2008JC004918.
- , and Coauthors, 2011: Implementation of the Coupled Ocean–Atmosphere Response Experiment flux algorithm with CO₂, dimethyl sulfide, and O₃. *J. Geophys. Res.*, **116**, C00F09, doi:10.1029/2010JC006884.
- Fan, Y., S. Lin, I. M. Held, Z. Yu, and H. L. Tolman, 2012: Global ocean surface wave simulation using a coupled atmosphere–wave model. *J. Climate*, **25**, 6233–6252, doi:10.1175/JCLI-D-11-00621.1.
- , I. M. Held, S. Lin, and X. Wang, 2013: Ocean warming effect on surface gravity wave climate change for the end of the twenty-first century. *J. Climate*, **26**, 6046–6066, doi:10.1175/JCLI-D-12-00410.1.
- , S.-J. Lin, S. M. Griffies, and M. A. Hemer, 2014: Simulated global swell and wind-sea climate and their responses to anthropogenic climate change at the end of the twenty-first century. *J. Climate*, **27**, 3516–3536, doi:10.1175/JCLI-D-13-00198.1.
- Gill, A., 1973: Circulation and bottom water formation in the Weddell Sea. *Deep-Sea Res.*, **20**, 111–140.
- Gnanadesikan, A., and Coauthors, 2006: GFDL’s CM2 global coupled climate models. Part II: The baseline ocean simulation. *J. Climate*, **19**, 675–697, doi:10.1175/JCLI3630.1.
- Gong, D., and S. Wang, 1999: Definition of Antarctic Oscillation index. *Geophys. Res. Lett.*, **26**, 459–462, doi:10.1029/1999GL900003.
- Griffies, S. M., 2009: Elements of MOM4p1. GFDL Ocean Group Tech. Rep. 6, 377 pp. [Available online at http://data1.gfdl.noaa.gov/~arl/pubrel/o/old/doc/mom4p1_guide.pdf.]
- , and Coauthors, 2005: Formulation of an ocean model for global climate simulations. *Ocean Sci.*, **1**, 45–79, doi:10.5194/os-1-45-2005.
- Harcourt, R. R., and E. A. D’Asaro, 2008: Large-eddy simulation of Langmuir turbulence in pure wind seas. *J. Phys. Oceanogr.*, **38**, 1542–1562, doi:10.1175/2007JPO3842.1.
- Hasselmann, S., and Coauthors, 1988: The WAM model—A third-generation ocean wave prediction model. *J. Phys. Oceanogr.*, **18**, 1775–1810, doi:10.1175/1520-0485(1988)018<1775:TWMTGO>2.0.CO;2.
- Holm, D., 1996: The ideal Craik–Leibovich equations. *Physica D*, **98**, 415–441, doi:10.1016/0167-2789(96)00105-4.
- Jochum, M., and Coauthors, 2013: The impact of oceanic near-inertial waves on climate. *J. Climate*, **26**, 2833–2844, doi:10.1175/JCLI-D-12-00181.1.
- Jullion, L., S. C. Jones, A. C. Naveira Garabato, and M. P. Meredith, 2010: Wind-controlled export of Antarctic Bottom Water from the Weddell Sea. *Geophys. Res. Lett.*, **37**, L09609, doi:10.1029/2010GL042822.
- Killworth, P. D., 1979: On chimney formation in the ocean. *J. Phys. Oceanogr.*, **9**, 531–554, doi:10.1175/1520-0485(1979)009<0531:OFITO>2.0.CO;2.
- Lane, E. M., J. M. Restrepo, and J. C. McWilliams, 2007: Wave–current interaction: A comparison of radiation-stress and vortex-force representations. *J. Phys. Oceanogr.*, **37**, 1122–1141, doi:10.1175/JPO3043.1.
- Large, W. G., J. C. McWilliams, and S. C. Doney, 1994: Ocean vertical mixing: A review and model with a nonlocal boundary layer parameterization. *Rev. Geophys.*, **32**, 363–403, doi:10.1029/94RG01872.
- Li, M., and C. Garrett, 1993: Cell merging and the jet/downwelling ratio in Langmuir circulation. *J. Mar. Res.*, **51**, 737–769, doi:10.1357/0022240933223945.
- Marshall, J., and F. Schott, 1999: Open-ocean convection: Observations, theory, and models. *Rev. Geophys.*, **37**, 1–64, doi:10.1029/98RG02739.

- McWilliams, J. C., and J. Restrepo, 1999: The wave-driven ocean circulation. *J. Phys. Oceanogr.*, **29**, 2523–2540, doi:10.1175/1520-0485(1999)029<2523:TWDOC>2.0.CO;2.
- , and P. P. Sullivan, 2000: Vertical mixing by Langmuir circulations. *Spill Sci. Technol. Bull.*, **6**, 225–237, doi:10.1016/S1353-2561(01)00041-X.
- , and B. Fox-Kemper, 2013: Oceanic wave-balanced surface fronts and filaments. *J. Fluid Mech.*, **730**, 464–490, doi:10.1017/jfm.2013.348.
- , P. P. Sullivan, and C.-H. Moeng, 1997: Langmuir turbulence in the ocean. *J. Fluid Mech.*, **334**, 1–30, doi:10.1017/S0022112096004375.
- , J. Restrepo, and E. Lane, 2004: An asymptotic theory for the interaction of waves and currents in coastal waters. *J. Fluid Mech.*, **511**, 135–178, doi:10.1017/S0022112004009358.
- Meredith, M. P., P. L. Woodworth, C. W. Hughes, and V. Stepanov, 2004: Changes in the ocean transport through Drake Passage during the 1980s and 1990s, forced by changes in the southern annular mode. *Geophys. Res. Lett.*, **31**, L21305, doi:10.1029/2004GL021169.
- Milly, P. C. D., and A. B. Shmakin, 2002: Global modeling of land water and energy balances. Part I: The land dynamics (LaD) model. *J. Hydrometeorol.*, **3**, 283–299, doi:10.1175/1525-7541(2002)003<0283:GMOLWA>2.0.CO;2.
- Polton, J. A., and S. E. Belcher, 2007: Langmuir turbulence and deeply penetrating jets in an unstratified mixed layer. *J. Geophys. Res.*, **112**, C09020, doi:10.1029/2007JC004205.
- , D. M. Lewis, and S. E. Belcher, 2005: The role of wave-induced Coriolis–Stokes forcing on the wind-driven mixed layer. *J. Phys. Oceanogr.*, **35**, 444–457, doi:10.1175/JPO2701.1.
- Qiao, F., Y. Yuan, Y. Yang, Q. Zheng, C. Xia, and J. Ma, 2004: Wave-induced mixing in the upper ocean: Distribution and application to a global ocean circulation model. *Geophys. Res. Lett.*, **31**, L11303, doi:10.1029/2004GL019824.
- Rainville, L., C. M. Lee, and R. A. Woodgate, 2011: Impact of wind-driven mixing in the Arctic Ocean. *Oceanography*, **24**, 136–145, doi:10.5670/oceanog.2011.65.
- Raschle, N., and F. Ardhuin, 2013: A global wave parameter database for geophysical applications. Part 2: Model validation with improved source term parameterization. *Ocean Modell.*, **70**, 174–188, doi:10.1016/j.ocemod.2012.12.001.
- Sallee, J.-B., E. Shuckburgh, N. Bruneau, A. J. S. Meijers, T. J. Bracegirdle, and Z. Wang, 2013: Assessment of Southern Ocean mixed-layer depths in CMIP5 models: Historical bias and forcing response. *J. Geophys. Res.*, **118**, 1845–1862, doi:10.1002/jgrc.20157.
- Skyllingstad, E. D., and D. W. Denbo, 1995: An ocean large-eddy simulation of Langmuir circulations and convection in the surface mixed layer. *J. Geophys. Res.*, **100**, 8501–8522, doi:10.1029/94JC03202.
- , W. D. Smyth, and G. B. Crawford, 2000: Resonant wind-driven mixing in the ocean boundary layer. *J. Phys. Oceanogr.*, **30**, 1866–1890, doi:10.1175/1520-0485(2000)030<1866:RWDMIT>2.0.CO;2.
- Smith, J. A., 1998: Evolution of Langmuir circulation during a storm. *J. Geophys. Res.*, **103**, 12 649–12 688, doi:10.1029/97JC03611.
- , 1999: Observations of wind, waves, and the mixed layer: The scaling of surface motion. *Wind-Driven Air–Sea Interface: Electromagnetic and Acoustic Sensing, Wave Dynamics, and Turbulent Fluxes*, M. L. Banner, Ed., University of New South Wales, 231–238.
- Smyth, W. D., E. D. Skyllingstad, G. B. Crawford, and H. Wijesekera, 2002: Nonlocal fluxes and Stokes drift effects in the *K*-profile parameterization. *Ocean Dyn.*, **52**, 104–115, doi:10.1007/s10236-002-0012-9.
- Sullivan, P. P., J. C. McWilliams, and W. K. Melville, 2007: Surface gravity wave effects in the oceanic boundary layer: Large-eddy simulation with vortex force and stochastic breakers. *J. Fluid Mech.*, **593**, 405–452, doi:10.1017/S002211200700897X.
- , L. Romero, J. C. McWilliams, and W. K. Melville, 2012: Transient evolution of Langmuir turbulence in ocean boundary layers driven by hurricane winds and waves. *J. Phys. Oceanogr.*, **42**, 1959–1980, doi:10.1175/JPO-D-12-025.1.
- Thompson, D. W. J., and J. M. Wallace, 2000: Annular modes in the extratropical circulation. Part I: Month-to-month variability. *J. Climate*, **13**, 1000–1016, doi:10.1175/1520-0442(2000)013<1000:AMITEC>2.0.CO;2.
- Tolman, H. L., 1998: Validation of a new global wave forecast system at NCEP. *Ocean Wave Measurements and Analysis*, B. L. Edge and J. M. Helmsley, Eds., ASCE, 777–786.
- Van Roekel, L. P., B. Fox-Kemper, P. P. Sullivan, P. E. Hamlington, and S. R. Haney, 2012: The form and orientation of Langmuir cells for misaligned winds and waves. *J. Geophys. Res.*, **117**, C05001, doi:10.1029/2011JC007516.
- Weijer, W., and Coauthors, 2012: The Southern Ocean and its climate in CCSM4. *J. Climate*, **25**, 2652–2675, doi:10.1175/JCLI-D-11-00302.1.
- Webb, A., and B. Fox-Kemper, 2011: Wave spectral moments and Stokes drift estimation. *Ocean Modell.*, **40**, 273–288, doi:10.1016/j.ocemod.2011.08.007.
- Winton, M., 2000: A reformulated three-layer sea ice model. *J. Atmos. Oceanic Technol.*, **17**, 525–531, doi:10.1175/1520-0426(2000)017<0525:ARTLSI>2.0.CO;2.